Solution Set Augmentation for Knee Identification in Multiobjective Decision Analysis

Guo Yu, Yaochu Jin, Markus Olhofer, Qiqi Liu, Wenli Du

2023

Preprint:

This is an accepted article published in IEEE Transactions on Cybernetics. The final authenticated version is available online at: https://doi.org/10.1109/TCYB.2021.3125071

Solution Set Augmentation for Knee Identification in Multiobjective Decision Analysis

Guo Yu, *Member, IEEE,* Yaochu Jin, *Fellow, IEEE,* Markus Olhofer, Qiqi Liu, Wenli Du

DOI: 10.1109/TCYB.2021.3125071

Solution Set Augmentation for Knee Identification in Multiobjective Decision Analysis

Guo Yu, *Member, IEEE,* Yaochu Jin, *Fellow, IEEE,* Markus Olhofer, Qiqi Liu, Wenli Du

***Abstract*—In multiobjective decision-making, most knee identification algorithms implicitly assume that the given solutions are well distributed and can provide sufficient information for identifying knee solutions. However, this assumption may fail to hold when the number of objectives is large or when the shape of the Pareto front is complex. To address the above issues, we propose a knee-oriented solution augmentation (KSA) framework that converts the Pareto front into a multimodal auxiliary function whose basins correspond to the knee regions of the Pareto front. The auxiliary function is then approximated using a surrogate and its basins are identified by a peak detection method. Additional solutions are then generated in the detected basins in the objective space and mapped to the decision space with the help of an inverse model. These solutions are evaluated by the original objective functions and added to the given solution set. To assess the quality of the augmented solution set, a measurement is proposed for verification of knee solutions when the true Pareto front is unknown. The effectiveness of KSA is verified on widely used benchmark problems and successfully applied to a hybrid electric vehicle controller design problem.**

***Index Terms*—Knee point identification, solution augmentation, inverse modeling, peak detection, multiobjective optimization.**

I. Introduction

In the real world, multiobjective optimization problems (MOPs) are very common and often involve multiple conflicting objectives [1]. Many multiobjective evolutionary algorithms (MOEAs) have been proposed to solve the MOPs [2]–[4], aiming to find a representative solution set of the Pareto optimal front (PoF) with a good balance between the convergence and diversity [5]. Different from these MOEAs, the preference-driven methods only seek to find segments of the PoF that satisfy the users' preferences [6]. The past decades have witnessed rapid research progresses of both approaches to multiobjective optimization in different areas such as the multicriteria decision making (MCDM) [7] and evolutionary multiobjective optimization (EMO) [8], [9].

However, several concerns have been raised regarding the preference-driven approach [10]. First, explicit preferences may be hard to be articulated beforehand, if the decision-maker (DM) does not have sufficient *a priori* knowledge of the problem. Second, it is not straightforward to articulate the preferences during the optimization, and interactively tuning the preferences during the optimization may be arduous and sometimes intractable. Third, it is resource-intensive in the *a posterior* approach to acquire a representative solution set over the whole PoF, especially when the number of objectives is large and the shape of the PoF is highly complex.

Accordingly, the search of naturally preferred solutions such as the knee points becomes attractive when the DM does not have sufficient *a priori* knowledge of the problems. The knee points are the solutions on the PoF, which need a large compromise in at least one objective to achieve a small amount of enhancement in other objectives [11]. It has also been shown that knee solutions contribute to a larger hypervolume in comparison with other Pareto optimal solutions [12]. In addition, knee points have been successfully used to deal with a wide range of problems, such as self-adaptive software [13], dynamic optimization [14], [15], many-objective optimization problems [16], sparse reconstruction [17], driving strategy for electric vehicles [18], compressing deep neural networks [19], subspace learning [20] and community detection [21].

Several methods for knee solution identification have been proposed. Branke et al. [11] apply the reflex angle to describe the convexity of the solutions along the PoF, and the solution with the largest reflex angle is regarded as the knee point. Based on the reflex angle, Deb and Gupta [22] propose a bend angle to characterize the knees. Following that idea, different angle-based methods are proposed [23], [24]. Another effective way for knee identification is to find out solutions having the maximum distance to the hyperplane constructed by the extreme points [12], [25], [26]. Branke et al. [11] define the expected marginal utility (EMU) with a set of weight vectors and the solutions with the highest utility are regarded as the knee candidates. An extension of EMU reported in [27] recursively uses the EMU to find the best knee candidates in the knee regions. In [28], [29] the dominance relationship is modified to search for the knee regions. The methods in [30], [31] use the min-max utility to find out knee candidates, where the solution in the knee region possesses the largest improvement per unit degradation. Other utility driven identification methods [32] have also been reported. Besides, a niching-based method [33] has been proposed to identify both convex and concave knee regions in two- or three-dimensional objective spaces. In addition, the research presented in [34] adopts a decomposition-based framework for approximating the knee solutions.

Guo Yu and Wenli Du are with the Key Laboratory of Smart Manufacturing in Energy Chemical Process, Ministry of Education, East China University of Science and Technology, Shanghai 200237, China. e-mail: {guoyu; wldu}@ecust.edu.cn.

Yaochu Jin is with the Chair of Nature Inspired Computing and Engineering, Faculty of Technology, Bielefeld University, D-33615 Bielefeld, Germany. He is also with the Department of Computer Science, University of Surrey, Guildford, Surrey GU2 7XH, UK. e-mail: yaochu.jin@uni-bielefeld.de. (*Corresponding author*)

Qiqi Liu are with the Department of Computer Science, University of Surrey, Guildford, Surrey GU2 7XH, UK. e-mail: qiqi.liu@surrey.ac.uk

Markus Olhofer is with Honda Research Institute Europe GmbH, D-63073 Offenbach/Main, Germany. e-mail: markus.olhofer@honda-ri.de.

Existing identification methods may have good performance in characterizing the knee candidates among a large number of solutions when the given solution set is well converged and well distributed in the knee regions. However, it is challenging to acquire a sufficiently large set of solutions to represent the entire PoF for problems having a large number of objectives due to the limited computing resources [10]. Accordingly, the performance of most knee identification algorithms will seriously degrade if the given solution set has a very small number of solutions distributed in a knee region.

Another challenge is how to verify the knee candidates in real-world optimization problems, whose PoFs is unknown and may be highly complex. To the best of our knowledge, no measurement has been proposed to verify the obtained knee candidates when the true Pareto front is unknown, although different identification methods have been proposed to acquire the knee candidates among solution sets.

The contributions of this paper are summarized as follows.

1) A framework consisting of auxiliary function construction, peak detection, and inverse mapping is proposed to augment a given solution set by generating additional promising solutions in the knee regions, thereby improving the quality of the identified knee solutions.
2) A novel method assisted by boxplots is suggested for verification of the knee candidates when the true Pareto front is unknown.

The rest of the paper is organized as follows. Section II presents the related definitions. The motivation and details of the proposed framework for augmenting the solution set are presented in Section III. Section IV demonstrates the effectiveness of the framework on a number of test instances and a real application. Finally, Section V concludes the paper.

II. Related Definitions

In this section, related definitions of multiobjective optimization, knee point, and multimodal optimization are given.

Definition 1 (*Multiobjective optimization problem*) Without loss of generality, a multiobjective optimization problem (MOP) can be formulated as the minimization of m objectives:

$$\begin{aligned} &\textit{minimize } \mathcal{F}(\mathbf{x}) = (f_1(\mathbf{x}), \cdots, f_m(\mathbf{x}))^T, \\ &\textit{s.t.} \quad \mathbf{x} \in \mathbb{X}, \quad \mathcal{F} \in \mathbb{Y}, \end{aligned} \tag{1}$$

where $\mathbf{x} = (x_1, \cdots, x_n)$ is the decision vector. $\mathbb{X} \subseteq \mathbb{R}^n$ is the decision space, and n is the number of decision variables. $\mathcal{F} : \mathbb{X} \to \mathbb{Y}$ consists of m objectives. $\mathbb{Y} \subseteq \mathbb{R}^m$ is the objective space.

Definition 2 (*Knee point*) A knee point of a PoF is defined as the solution having the maximum distance to the convex hull of individual minima (CHIM) [25] constructed by the extreme points.

$$\mathbf{x} = \arg\max_{\mathbf{x}} d(\mathcal{F}(\mathbf{x}), S). \tag{2}$$

where CHIM is defined as follows. Let $\mathbf{x_i}^*$ be the global minimum of $f_i(\mathbf{x})$. Let Φ be an $m * m$ matrix whose i^{th} column is $f_i(\mathbf{x_i}^*) - f_i(z^*)$, $i = 1, \ldots, m$, where z^* is the ideal point. Let $B = \{\beta : \beta \in \mathbb{R}^m, \sum_{i=1}^{m} \beta_i = 1, \beta_i \geq 0\}$, then the set of points in $\mathbb{R}^m$ that are convex combinations of $f_i(\mathbf{x_i}^*) - f_i(z^*)$, i.e., $\{\Phi\beta : \beta \in B\}$, is referred to as the convex hull of individual minima (CHIM). The reader is referred to [25] for more details.

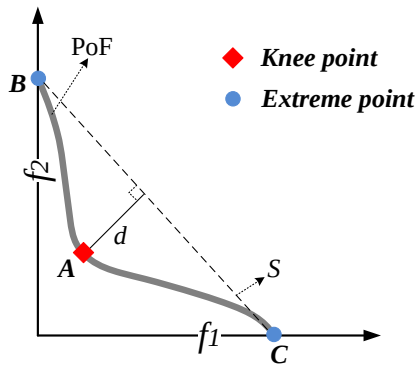

Fig. 1. An example of a knee point (A) of a PoF. Points B and C are the extreme points. d is the distance from point A to the hyperplane S constructed by the extreme points.

In Fig. 1, solution A is the knee as it has the largest distance d to the hyperplane S.

Definition 3 (*Multimodal optimization problem*) Without loss of generality, a multimodal single-objective optimization problem (MMOP) involving multiple minimums can be formulated as the minimization of an objective function:

$$\begin{aligned} &\textit{minimize } f(\mathbf{x}), \\ &\textit{s.t. } \mathbf{x} \in X, \end{aligned} \tag{3}$$

where $f(\mathbf{x})$ is the objective function, and $\mathbf{x} = (x_1, \cdots, x_n)$ is the decision vector, and n is number of decision variables.

III. Proposed Framework

In this section, the motivation of the paper is introduced. Then a novel knee solution augmentation (KSA) framework is proposed for augmenting solutions for given a set of approximated Pareto optimal solutions, followed by a description of the main components of KSA.

A. Motivation

Conventional MOEAs aim to find a solution set to represent the PoF with a good balance between the convergence and diversity. After that, the DM is asked to select his or her preferred solutions among the given solution set. However, sometimes it is challenging to require the DM to explicitly specify his or her preferences when the DM does not have sufficient *a priori* knowledge about the distribution of the Pareto optimal solutions. Therefore, it is of practical interest to identify the naturally preferred solutions such as the knee solutions in such situations.

However, several factors may prevent the acquisition of a well distributed representative solution set of the PoF, due to, e.g., a limited size of population, the very large number of the objectives of the MOPs, the complexity of the PoF, and a limited amount of computing resources [10]. Unfortunately,

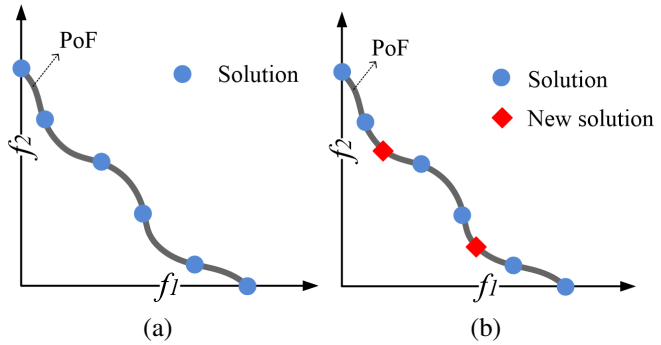

Fig. 2. An example illustrating the motivation of the work. (a) The obtained Pareto optimal solutions denoted by dots and the Pareto front denoted by the curve. (b) Two augmented solutions denoted by diamonds, which are helpful for identifying knee points of the PoF.

most research implicitly assumes that the given solution set is able to provide sufficient information for identifying all knee solutions, which is not always true. For example, six solutions are evenly distributed on the PoF in Fig. 2 (a), but none of them are good knee candidates. In this situation, even a diverse solution set on the PoF is not necessarily able to provide high-quality knee solutions. However, *a priori* knee-oriented methods are not always effective in finding knee candidates, especially on problems having discontinuous PoF and are multimodal, as empirically demonstrated in Section I of the Supplementary material. This motivates us to enhance the quality of the given solution set by generating new solutions in the promising knee regions according to the information provided by the given solutions. Typically we can allocate a certain amount of computing budget for targeting solutions in the promising knee regions rather than achieving an evenly distributed solution set of the whole PoF. For example, Fig. 2 (b) shows that two new solutions (denoted by the diamonds) can be generated to augment the solution set that are most beneficial for knee identification.

To augment the solution set by generating new candidate knee solutions, a meta-model that approximates the auxiliary function may be helpful, now that an analytical form of the auxiliary function is unavailable. Note that meta-models have been widely used in evolutionary optimization, in particular in surrogate-assisted evolutionary optimization of expensive problems [35], [36], or more generally, in data-driven evolutionary optimization [37]. Surrogates may be adopted to directly approximate the expensive objective functions [38], scalarizing functions [39], [40], or the hypervolume contribution of a solution [41]. Alternatively, surrogates may also be used as a classifier to distinguish dominated or non-dominated solutions [42], learn the rank of the solutions [43], [44], or learn the dominance relationship between the solutions [45], [46]. Interestingly, Giagkiozis and Fleming [47], [48] build an inverse model that maps the PoF to PoS to generate non-dominated solutions from the PoF. Cheng *et al.* [49] decompose a multivariate inverse model into a number of univariate inverse models to replace the genetic operators to generate solutions. In the present work, we also introduce an inverse model to help generate solutions in potential knee regions, in addition to the meta-model approximating the auxiliary function.

B. Knee solution augmentation

The main framework of knee solution augmentation (KSA) is presented in Algorithm 1. We assume that a Pareto optimal (or non-dominated) solution set P is obtained by an MOEA. Then, KSA starts a repeated procedure for solution augmentation. The procedure consists of the following main steps. First, normalize the population P according to Eq. 4. Then, an inverse model that builds a functional map from the objective space to the decision space is trained based on the existing solution set. Afterwards, KSA transforms the approximated Pareto (non-dominated) front into a multimodal auxiliary function, whose minimums of the basins correspond to the knee points and the basins to the knee regions of the Pareto front. This transformation makes it possible for KSA to employ any peak detection algorithm [50] to efficiently locate knee regions or knee points of the Pareto front by finding the minimums or basins of the multimodal auxiliary function. Note, however, that the true auxiliary function is not available and therefore a surrogate model must be built based on the given solutions to approximate the auxiliary function. Hence, the next step is to build a meta-model to approximate the auxiliary function. In this work, Kriging model [51] is adopted as the meta-model. A peak detection algorithm [50] is then adopted to find solutions in the potential knee regions, i.e., the basins of the approximated auxiliary function. The last step is to update the population with the obtained potential knee candidates.

The main components of KSA as listed in Algorithm 1 will be detailed in the following and the analysis of computational complexity is provided in Section VI of the Supplementary material.

Algorithm 1 Knee-oriented solution augmentation (KSA)

Input : Given solution set: P,number of objectives: m.
Output: Output solution set: P

while *Termination condition is not satisfied* **do**
  Normalization: Get the normalized objective values $\bar{F} = (\bar{f}_1, \ldots, \bar{f}_m)$ of each solution $\mathbf{x}$ in P.
  Inverse Model Training: Train an inverse model (e.g., RBFNNs [47]) mapping the normalized objective values ($\bar{F}$) to the decision vectors ($\mathbf{x}$) of P.
  Multimodal Auxiliary Function Transformation: Do multimodal transformation on P to transform the solutions from P into the points on a multimodal auxiliary function.
  Meta-model Building: Build meta-model to fit the multimodal auxiliary function.
  Peak Detection based Knee Search: Apply the peak detection based knee search to find the minimums (Q) of the estimated auxiliary function.
  Update: Get the decision vectors $\mathbf{x}^{'}$ of Q via RBFNNs and evaluate Q by the true objective functions: $Q = \mathcal{F}(\mathbf{x}^{'})$, then update P with Q.
end
Return P

C. Inverse model

Before the construction of the inverse model, the solutions are normalized. The normalized objective values $\bar{F} = (\bar{f}_1, \ldots, \bar{f}_m)$ of a solution $\mathbf{x}$ in P are obtained as follows.

$$\bar{f}_i(\mathbf{x}) = \frac{f_i(\mathbf{x}) - f^i_{min}}{f^i_{max} - f^i_{min}}. \tag{4}$$

where $f_i(\mathbf{x})$ and $\bar{f}_i(\mathbf{x})$ are the i-th objective and normalized objective values of solution $\mathbf{x}$, $f^i_{min} = \min_{\forall \mathbf{x} \in P}\{f_i(\mathbf{x})\}$, and $f^i_{max} = \max_{\forall \mathbf{x} \in P}\{f_i(\mathbf{x})\}$.

Given a normalized solution set X and its normalized objective values $\bar{F} = (\bar{f}_1(X), \cdots, \bar{f}_m(X))$ in Eq. 4, an inverse model [47] is trained on the solution set to learn the functional mapping from the objective space to the decision space.

The procedure of the inverse modeling is given as follows.

Step 1:Do orthographic projection on $\bar{F}$ to get its projection $\tilde{F}$ on a hyperplane $\bar{F}_E$, i.e., $\tilde{F} = \bar{F}\bar{F}^T_E$, where $\bar{F}_E = H(H^T H)^{-1} H^T$, and $H = (e_1 - 1/m, \ldots, e_{m-1} - 1/m)$. m-1 unit vectors are acquired like $\{e_1, \ldots, e_{m-1}\}$, where $e_i = (0, \ldots, 0, 1, 0, \ldots, 0)$, and one is set in the i-th position. m is the number of objectives.

Step 2:Normalize $\tilde{F}$ with the similar operation in *Step 1*.

Step 3:Build radial basis function neural networks (RBFNNs) using the Gaussian basis function [52], where the input and output are $\tilde{F}$ and X, respectively.

After the training of the inverse model, the value of decision vectors of a solution can be obtained, when its objective values are given.

D. Multimodal auxiliary function transformation

The multimodal auxiliary function transformation aims to transform a PoF into a multimodal function (in Eq. 3). According to the definition of the knee in [25], the knee is characterized with the local maximum distance from solution to the hyperplane constructed by the extreme points. Each convex hull of individual minima (CHIM) is correlated to a valley of a multimodal function, termed auxiliary function here, in which the independent variables of the function are the objective functions, and dependent variable is the negative distance from the solutions to the hyperplane constructed by the extreme points.

Specifically, transformation of the PoF into the auxiliary function is achieved as follows. The normalized objective values of a solution p can be obtained by Eq. 4, $(\bar{f}_1(p), \cdots, \bar{f}_m(p))$, and is then transformed into the fitness value $(FV(p))$ of the multimodal auxiliary function in the following way

$$FV(p) = \frac{\bar{f}_1(p) + \cdots + \bar{f}_m(p) - 1}{|\overrightarrow{\mathfrak{n}}|}, \tag{5}$$

where $\overrightarrow{\mathfrak{n}} = (1, \ldots, 1)$ is the normal vector of the hyperplane $S : \bar{f}_1 + \cdots + \bar{f}_m = 1$.

Fig. 3 presents an illustrative example of a Pareto front and the corresponding transformed auxiliary function, showing that the minimums of the multimodal auxiliary function that correspond to the knee points of the PoF.

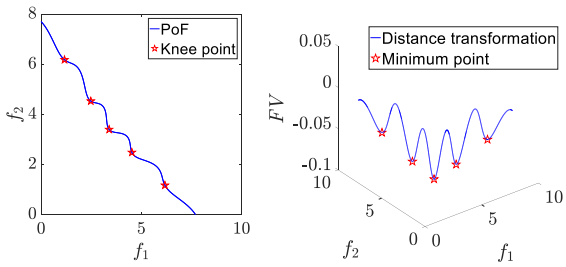

Fig. 3. (a) The PoF of DEB2DK [11] is presented and the corresponding fitness curve of the PoF is obtained after the multimodal transformation. (b) The transformed multimodal function, whose minimums correspond to the knee points of PoF.

Algorithm 2 Peak detection based knee search

Input : Transformed solution set: $P : [p^1, \cdots, p^N]$, corresponding fitness values: $\{FV\}$, the Kriging model: M_{model}, number of objectives: m.
Output: Output solution set: Q

$Q = \emptyset$
Find knee candidates (i.e., $Peaks$) by peak detection (PD) [50] in terms of FV.
foreach $l = 1 : |Peaks|$ **do**
  $I_{best} = findIndex(Peaks(l))$ // find the index of $Peaks(l)$ from P and assign it to I_{best}.
  foreach $i = 1 : N$ **do**
    $p^v = p^{I_{best}} + F \cdot (p^{r_1} - p^{r_2})$
    $j_{rand} = randi([1, m])$
    offspring$(i) = p^i$
    foreach *j=1:m* **do**
      if $rand <= CR || j = j_{rand}$ **then**
        offspring$(i).f_j = p^v.f_j$
      end
    end
    [μ(offspring(i)),s(offspring(i))] = M_{model}(offspring(i))
    LCB_i = μ(offspring(i)) - ωs(offspring(i))
  end
  $index$ = Sort(LCB,'ascend');
  $Q = Q \cup$offspring$(index(1))$
end
Return Q

E. Meta-model

After the transformation of the population, discrete points of the multimodal auxiliary function are acquired. Hence, a meta-model is built to fit the multimodal auxiliary function by using the transformed solutions and estimate the FV value. The Kriging model [51] is chosen as the meta-model, mainly because the Kriging model is able to provide uncertainty information for the estimated values.

Given a solution q in the objective space, the FV value of q is approximated by the Kriging model:

$$FV(q) = \mu(q) + s^2(q), \tag{6}$$

where $\mu(q)$ is the prediction value of a stochastic process. $s(q)$ is a zero mean stationary Gaussian distribution. $N(\mu(p), s^2(p))$ is regarded as a predictive distribution for $FV(p)$ on the basis of training data (Q, FV). This work adopts the DACE toolbox [53] to train the Kriging model.

F. Search of knees based on peak detection

The peak detection based knee search is proposed to generate solutions in the possible knee regions and search for the knee candidates, after the training of the meta model. In this approach, the differential evolution (DE) operators [54] assisted by a peak detection [50] are applied for generating solutions with the help of the approximated multimodal auxiliary function, and the candidate knee solutions are selected according to the lower confidence bound (LCB) [55], $LCB(p) = \mu(p) - \omega\, s(p)$, where $\mu(p)$ is the expected objective value of solution p, $s(p)$ is the uncertainty level of the estimated objective value, and ω is a hyperparameter. Following [55], [56], ω is set to 2 in this work. Note that LCB is adopted as the acquisition function to measure the quality of a new solution p, mainly because it can take into account the balance between exploitative search in promising regions with a low $\mu(p)$ and exploratory search with a high $s(p)$.

The peak detection based knee search is detailed in Algorithm 2. In Line 11, peak detection [50] is adopted to find the knee candidates (peaks) in the current solution set P, where the peaks are the knee candidates among P. After that, Lines 14 – 24 describe the generation of solutions (a set of offspring) and Lines 25 – 26 the selection of potential knee candidates in the offspring set. During the generation of solutions, the mutation and crossover operators in DE are adopted to generate solutions around the peak solutions or in potential knee regions. Specifically, a peak solution $p^{I_{best}}$ is introduced into the mutation in Line 15, and p^{r_1} and p^{r_2} are two randomly selected solutions from P. As a result, the base solution p^v is obtained and $F \in (0, 2]$ is a scaling factor. After the operation of mutation, then the crossover operation is conducted on the base solution as shown from Lines 18 – 22. If the condition $rand <= CR || j = j_{rand}$ is satisfied, the jth objective value of the offspring will be replaced with that of the base solution and $j = 1, \cdots, m$. $CR \in [0, 1]$ is a constant crossover rate. Following [54], both F and CR are set to 0.8. Once new solutions are generated, they are forwarded to the Kriging model (Line 23) to get their LCB values (in Line 23). Finally, the new solutions will be sorted according to the LCB values in an ascending order (Line 25) and the best one with the smallest LCB value will be added into the output solution set (Line 26). Accordingly, the new solutions with a smaller LCB value will be selected with a higher priority. Note that there may be three situations in which solutions have a small LCB value. 1) The solutions are located close to the minimums of the multimodal auxiliary function, and as a result, they have a small expected FV value (s). 2) The solutions are located in a knee region but far away from the knees, because they have a small LCB value that combines the expected FV value (μ) with the uncertainty (s). 3) The solutions are located in an unexplored knee region, resulting in a large uncertainty level (s). Thus, it is helpful to use the LCB as the criterion for identification of knee solutions.

G. Update operation

After the operation of solution generation, the selected promising solutions are used to update the given solution set.

The details of the update operation are presented in Algorithm 3. For each solution q from the new solution set Q, it is forwarded to the pre-trained inverse model (RBFNNs) to get its decision vector values $\mathbf{x}(q)$ as shown in Line 30. Once the decision variable values of the new solutions are obtained, they are evaluated by using the objective functions (in Line 31). After that, the obtained solution set Q is merged with the given solution set P via the Pareto dominance relationship, as described in Lines 33. Specifically, only the non-dominated solutions are kept in the updated solution set P.

Algorithm 3 Update operation

Input : Selected promising solution set: Q, the given population and corresponding decision vectors (P, D), the pre-trained inverse model: RBFNNs.
Output: P

29 **foreach** $q \in Q$ **do**
30 Get values of the decision variables $\mathbf{x}$ via RBFNNs.
31 Get objective values of q by $\mathcal{F}(\mathbf{x})$ in Eq. 1.
32 **end**
33 Update P with Q.
34 **Return** P

IV. Experiments and discussions

A. Experimental settings

To test the effectiveness of the proposed framework and identification method, widely used knee-oriented benchmark problems are adopted for empirical studies in this work, including DO2DK [11], DEB2DK [11], CKP [33], DEB3DK [11], and the PMOP test suite[1] [57] with six diverse knee functions which control the features of the knee regions. The settings of the problems are presented in Table I, where 'asymmetric' and 'symmetric' denote whether the PoF is asymmetrical or not. Nondifferentiable means that the knee is nondifferentiable. Unimodal and multimodal describe the difficulty in convergence. Discontinuous means that the PoF is disconnected. Basic shapes are the PoFs which the knee functions are embedded into to create the knee regions [57]. The allowed maximum number of generations and fitness evaluations are the stopping criterion for the optimizer and the proposed framework (KSA)[2], respectively.

Peak detection (PD) in [50] is originally designed to find the maximums of maximization multimodal problems. In this study, we adopt PD for knee identification (PD-KI) on solution sets with the help of the multimodal auxiliary function transformation proposed in subsection III-D. Three representative knee identification methods are taken into account in the

[1]https://github.com/GYResearch/PMOPs-Benchmark.
[2]https://github.com/GYResearch/KSA-test.

comparative studies, including the KnEA [12], EMU^r [27], TKR [30]. Specifically, KnEA identifies the knees based on the distance to hyperplane constructed by the extreme points, where the parameter 'rate' is suggested to set to 0.5 for knee identification [12]. EMU^r recursively uses the expected marginal utility to search for the knee candidates, where the number of weight vectors is set to 100, 105, 126, and 156 for two-, three-, five- and eight-objective problems, respectively. TKR searches for knees by using a ratio between the gain and deterioration when the objectives of two solutions are exchanged, where a parameter ϵ is set to 0.001 as suggested in [30] for removing the duplicated solutions.

Two knee-driven indicators are applied for the evaluation of the results obtained by the proposed framework and knee identification methods, i.e., the knee-driven inverted generational distance (KIGD) [57] and the knee-driven dissimilarity (KD) [57]. In the comparative experiments, the Wilcoxon rank sum test (a significance level is set as 0.05) is adopted to analyze the KIGD and KD results (obtained by 20 independent runs), where "+", "-", and "≈" indicate that the result is significantly better, significantly worse and statistically comparable to the solutions obtained by PD-KI, respectively. All experiments are conducted on the platform for evolutionary multiobjective optimization (PlatEMO) [58].

Given a set of reference points $\mathcal{R}$ in the knee regions, and a set of true knee points $\mathcal{K}$, the KIGD and KD values of the obtained knee candidate set $\mathcal{P}$ are achieved as follows.

- The knee-driven inverted generational distance (KIGD) is defined as follows:

$$\text{KIGD} = \frac{1}{|\mathcal{R}|}\sum_{\iota=1}^{|\mathcal{R}|} dist(r_\iota, \mathcal{P}), \tag{7}$$

  where $dist(r_\iota, \mathcal{P})$ denotes the shortest Euclidean distance from reference point $r_\iota \in \mathcal{R}$ to the solution set $\mathcal{P}$.
- The knee-driven dissimilarity (KD) is presented as follows:

$$\text{KD} = \frac{1}{|K|}\sum_{\iota=1}^{|K|} dist(k_\iota, \mathcal{P}), \tag{8}$$

  where $dist(r_\iota, \mathcal{P})$ denotes the shortest Euclidean distance from knee point $r_\iota \in \mathcal{K}$ to the solution set $\mathcal{P}$.

The KIGD indicator evaluates both the proximity and the diversity of the obtained solution set covering the knee regions. KD mainly evaluates the accuracy and completeness of the obtained solution set by checking whether it contains at least one distinctive solution close to each true knee points.

Note that the reference points in the knee regions are generated in the following way as reported in [57]. The first step is to randomly sample a large number of Pareto optimal points and then use the k-nearest neighbor method introduced in SPEA2 [59] to remove the most crowded points one by one until the required size of reference points is left. Once a uniform set of reference points on the PF is obtained, the second step is to locate the feasible knee points and define a knee region for each knee point using a predefined radius. Finally, the reference points within the knee regions are kept as the final reference points. The reader is referred to [57] for the definition of the radius.

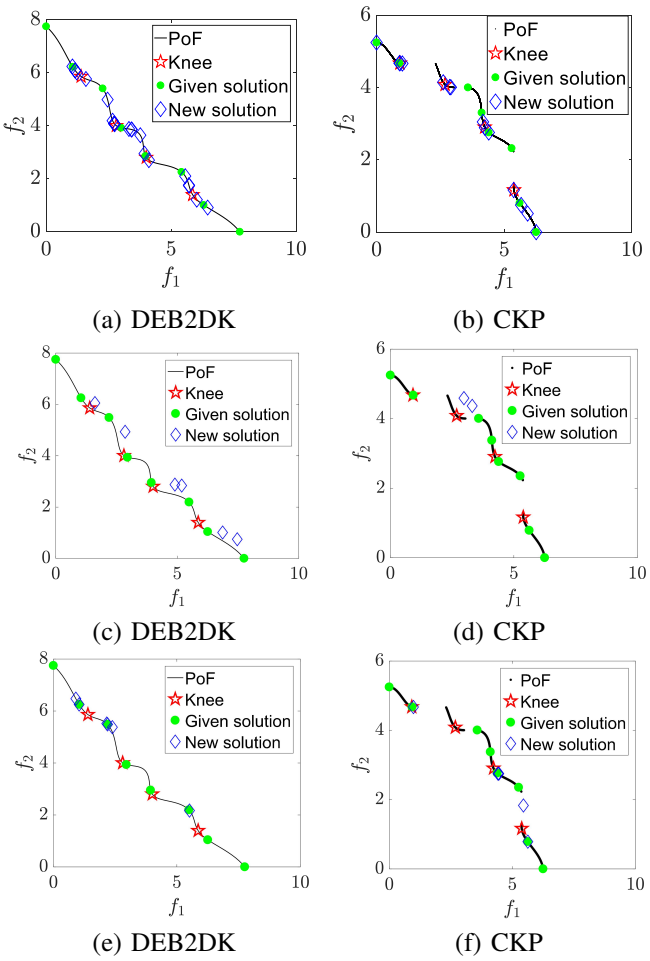

Fig. 4. Examples on DEB2DK [11] and CKP [33] problems to show the results based on KSA, random sampling, or genetic operators, where the given solutions are highlighted in green dots, and the new solutions are denoted by the blue diamonds.

Another indicator (denoted as increment) is adopted to evaluate the increment of the KIGD or KD values of the solution sets obtained before and after the augmentation by KSA.

$$Increment = \frac{V_{before} - V_{after}}{V_{before}} \tag{9}$$

where V_{before} and V_{after} are the indicator values (KIGD or KD values) of the obtained solution sets before (or without) and after (or with) the augmentation by KSA, respectively. A positive increment value means the augmented solution set has better performance than the solution set before (or without) the augmentation of KSA. The larger the increment, the better performance is achieved by KSA.

B. Pilot studies on KSA

In KSA, the inverse model based knee search is conducted to generate promising solutions in the potential knee regions. Here, a pilot study investigating the performance of KSA without the inverse model is conducted. Instead of using the inverse model, KSA uses random sampling or genetic operators to generate solutions around the potential peaks of DEB2DK [11] and CKP [33] under the condition that a

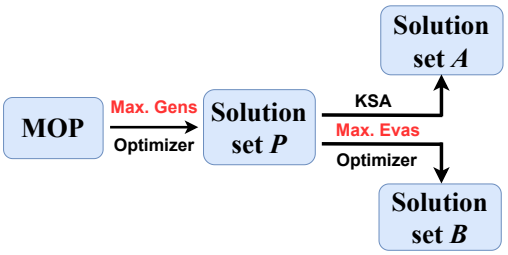

Fig. 5. An illustration of the experimental design, where Max.Gens and Max.Evas are the maximum number of generations and evaluations, respectively.

maximum of 25 fitness evaluations is allowed to augment the given solution set. Random sampling means to sample solutions around the peak solutions with Gaussian noise of zero mean and a standard deviation of 0.05 in the decision space. The genetic operators are the simulated binary crossover [60] and polynomial mutation [61] with the same distribution indexes of 20.

Figures 4 (a) and (b) present the results obtained by KSA on the two test problems. In these figures, most new solutions (denoted by blue diamonds) are located closer to the knees (red stars) than the given solutions (green dots) on different PoFs. Furthermore, some new solutions are generated in the unexplored knee region where the value of f_2 is around 4.0 in Fig. 4 (b). Clearly, the quality of the solution set has been greatly improved. The result indicates that KSA can learn the structure of the PoF and is able to generate solutions in potential knee regions.

Figures 4 (c) and (d) plot the new solutions generated by random sampling. The results show that only two and six non-dominated solutions, respectively, are generated for DEB2DK and CKP. Besides, most solutions have poor convergence since they are located far away from the PoF. These results indicate that random sampling fails to effectively generate promising solutions in the potential knee regions, even if the Gaussian noise is small.

The augmented solutions obtained by random sampling and genetic operators are given in Figs. 4 (e) and (f). The results show that the new solutions are located close to the given solutions and very few of them are close to the true knees. These results show that the the genetic operators are incapable of producing good solutions in the potential knee regions.

In summary, KSA outperforms random sampling and the genetic operators in producing promising solutions around the potential knee regions.

C. Comparative experiments on KSA and PD-KI

An illustration of the experimental design is given in Fig. 5. For a fair comparison, all experiments are conducted with the same number of evaluations. Both solution sets (A and B) are taken from the same parent solution set P, where P is obtained by running RVEA for a maximum number of generations. However, A and B are generated in different ways. Specifically, A is obtained by KSA, while solution set B is generated by further optimizing P using RVEA with the same number of fitness evaluations used by KSA. During the comparison, PD-KI identifies the knee candidates in the solution set A. Other identification methods follow the conventional framework to search the knee candidates in solution set B.

1) Analysis on KIGD results: In this section, the analysis on the KIGD results are presented in terms of Table II and Table III.

Table II exhibits the KIGD results on 32 instances. The best results highlighted in grey show that PD-KI ranks the first with 20 best records, followed by KnEA and EMU^r with 7 and 5 best records, respectively. Moreover, PD-KI outperforms others on most problems in terms of the rank sum values. Specifically, TKR loses on 29 out of 32 instances. EMU^r loses its advantages on 23 instances and wins on 9 out of 32 instances. Similar results can be seen on KnEA. Especially, PD-KI is competitive in identifying the knee regions on CKP, DO2DK, DEB2DK, PMOP1, PMOP7 and PMOP10 problems. Since these problems are relatively easier to be optimized, hence the inverse model can get more accurate estimation of the structure of the Pareto front. In other words, the results indicate that KSA is able to improve the performance of the solution set on most instances. However, PD-KI loses its advantages on multimodal problems such as PMOP3 and PMOP4 with many asymmetrical knee regions, which are hard to knee identification by PD. Hence, KSA performs worse on these problems. Overall, PD-KI performs better in terms of diversity than other identification methods given the same number of evaluations.

Table III shows the KIGD indicator values and corresponding increment values obtained by the identification methods based on the augmented solution set (A) provided by KSA. Specifically, the first column of the increment values in Table III shows how much the improvement of the KIGD values of the solution sets (A) obtained by KSA over the solution set (B) obtained by the optimizer (RVEA). The results indicate that the increment is positive ($\uparrow$) in 28 out of 32 test cases, suggesting that the compared knee identification algorithms are able to achieve more diverse solutions in the knee regions from the solution sets augmented by KSA. For example, KnEA has achieved the best result on 14 test instances and improved results on 20 instances compared to those in Table II without data augmentation. The overall performances of EMU^r and TKR are also improved, as both achieved better results on 23 out of 32 test instances. From the above results, we can conclude that KSA can improve the performance of other identification methods by providing more diverse solutions in the knee regions, which is also verified in Section IV of the Supplementary material.

However, some increment values in Table III are negative. The negative values of the performance indicators of the solution sets mainly occur on PMOP4, which is highly multimodal and has a complex asymmetrical PoF. In Section III of the Supplementary material, we also present some additional experimental results showing that an increase of the proximity of the population will improve the performance of KSA in producing promising knee candidates in the knee regions. When KSA fails to produce promising solutions in the knee regions, i.e., the augmented solutions are in the non-knee

TABLE I
EXPERIMENTAL SETTINGS.

Instances	No. of objectives (m)	No. of variables (n)	Size of Population (N)	Max. Generations	Parameters: $K, (A, B, s, p, l)$	Characteristics	No. of convex knees	Max. Evaluations
DO2DK	2	30	20	1000	$K = 3, 4$	Asymmetric, unimodal	K	100
DEB2DK	2	30	20	500	$K = 4, 5$	Symmetric, unimodal	K	100
CKP	2	30	20	500	$K = 4, 5$	Symmetric, discontinuous, unimodal	K	100
DEB3DK	3	30	50	500	$K = 2, 3$	Symmetric, discontinuous, unimodal	K^2	100
PMOP1	2,3,5,8	$m+9$	20,50,50,100	500,500,1000,1000	(4,1,-1,1)	Linear basic shape, symmetric, discontinuous, unimodal	$\lceil \frac{A}{2} \rceil^{m-1}$	150,150,150,200
PMOP3	2,3,5,8	$m+9$	20,50,50,100	500,500,1000,1000	(4,1,2,1)	Convex basic shape, symmetric, multimodal	$\lceil \frac{A}{2} \rceil^{m-1}$	150,150,150,200
PMOP4	2,3,5,8	$m+9$	50,50,50,100	1000,1000,2000,2000	(6,1,-1,1)	Concave basic shape, asymmetric, nondifferentiable, discontinuous, multimodal	$\lfloor \frac{A+1}{3} \rfloor^{m-1}$	150,150,150,200
PMOP6	2,3,5,8	$m+9$	20,50,50,100	500,500,1000,1000	(2,1,2,1)	Convex basic shape, symmetric, discontinuous, multimodal	$(A-1)^{m-1}$	150,150,150,200
PMOP7	2,3,5,8	$m+9$	20,50,50,100	500,500,1000,1000	(4,1,2,1)	Linear basic shape, symmetric, discontinuous, multimodal	$\lceil \frac{A}{2} \rceil^{m-1}$	150,150,150,200
PMOP10	2,3,5,8	$m+9$	50,50,50,100	1000,1000,2000,2000	(1,1,2,1,12)	Linear basic shape, asymmetric, multimodal	$(2*A)^{m-1}$	150,150,150,200

TABLE II
THE KIGD VALUES (AVERAGE VALUES, VARIANCE VALUES) OF THE CANDIDATE SOLUTION SETS OBTAINED BY THE IDENTIFICATION METHODS.

Instances	K	EMU^{r*}	TKR	KnEA	PD-KI
CKP	4	2.436E+00 (2.600E-05)−	3.220E+00 (3.257E-01)−	6.570E-01 (4.272E-03)−	1.351E-01 (1.009E-03)
	5	2.422E+00 (2.400E-05)−	2.655E+00 (8.034E-01)−	4.767E-01 (3.057E-03)−	1.427E-01 (5.100E-03)
DO2DK	3	1.073E+00 (1.562E-01)−	2.414E+00 (7.791E-01)−	8.621E-01 (1.514E-01)+	9.037E-01 (1.564E-01)
	4	9.801E-01 (1.245E-01)−	1.631E+00 (9.174E-02)−	8.049E-01 (1.572E-01)+	8.113E-01 (1.556E-01)
DEB2DK	4	6.002E-01 (8.624E-02)−	3.127E+00 (2.128E-03)−	6.349E-01 (9.889E-02)−	1.544E-01 (2.968E-03)
	5	1.122E+00 (4.369E-02)−	2.473E+00 (2.885E-01)−	6.818E-01 (1.092E-02)−	2.041E-01 (5.325E-03)
DEB3DK	2	4.243E+00 (2.234E-03)−	2.753E+00 (5.992E-01)−	2.159E+00 (2.280E+00)−	1.908E+00 (1.032E+00)
	3	3.941E+00 (5.560E-04)−	2.176E+00 (5.298E-01)−	3.267E+00 (4.026E+00)−	1.910E+00 (4.182E-01)
Instances	Obj.	EMU^{r*}	TKR	KnEA	PD-KI
PMOP1	2	8.011E-02 (0.000E+00)−	5.736E-01 (0.000E+00)−	5.895E-02 (0.000E+00)−	5.233E-02 (8.000E-06)
	3	3.597E-01 (3.600E-05)−	7.137E-01 (0.000E+00)−	2.441E-01 (0.000E+00)+	3.057E-01 (1.998E-03)
	5	2.654E+00 (1.651E-02)−	1.657E+00 (5.718E-02)−	1.161E+00 (1.000E-06)−	1.033E+00 (4.103E-02)
	8	4.474E+00 (3.449E-01)−	2.867E+00 (6.506E-01)−	7.201E+00 (1.941E+00)−	2.151E+00 (8.985E-02)
PMOP3	2	7.939E-01 (7.362E-01)−	2.196E+00 (1.836E+00)−	7.927E-01 (7.579E-01)−	1.621E+00 (1.028E+00)
	3	3.470E-01 (6.521E-03)+	1.079E+00 (3.293E-02)−	3.336E-01 (9.126E-03)+	9.267E-01 (5.173E-02)
	5	6.027E-01 (3.080E-03)+	9.168E-01 (1.405E-03)+	5.163E-01 (1.474E-02)+	2.150E+00 (2.375E-01)
	8	7.229E-01 (5.448E-03)+	9.034E-01 (1.515E-03)+	7.570E-01 (2.800E-01)+	4.942E+00 (1.071E+00)
PMOP4	2	2.986E+00 (2.794E+00)−	3.160E+00 (3.209E+00)−	1.842E+01 (4.971E+03)−	2.936E+00 (3.158E+00)
	3	4.321E+00 (5.875E+00)+	4.429E+00 (5.448E+00)+	3.846E+01 (8.940E+03)+	4.636E+00 (5.016E+00)
	5	1.242E+00 (1.302E-02)+	2.086E+00 (2.538E-01)−	1.305E+01 (2.441E+03)+	1.462E+00 (1.210E-01)
	8	2.845E+00 (3.891E-02)+	5.392E+00 (1.657E+00)−	3.848E+01 (9.908E+03)−	3.547E+00 (1.535E+00)
PMOP6	2	6.917E-01 (1.296E+00)+	2.254E+00 (4.626E+00)−	6.711E-01 (1.323E+00)+	7.361E-01 (1.526E+00)
	3	1.917E-01 (4.600E-04)+	6.612E-01 (3.149E-02)−	2.662E-01 (9.899E-02)+	3.330E-01 (2.915E-02)
	5	5.116E-01 (4.669E-03)+	7.529E-01 (7.299E-03)−	7.942E-01 (5.275E-01)−	5.787E-01 (3.037E-02)
	8	1.178E+01 (1.199E-01)−	1.478E+01 (1.439E+00)−	1.799E+01 (4.957E+01)−	9.572E+00 (1.872E+00)
PMOP7	2	8.657E-01 (1.924E-01)−	1.629E+00 (8.924E-02)−	1.179E+00 (1.319E-01)−	2.464E-01 (2.188E-02)
	3	7.257E-01 (1.340E-02)−	7.746E-01 (7.529E-03)−	6.664E-01 (8.441E-02)−	2.361E-01 (5.430E-03)
	5	6.237E-01 (2.056E-03)−	5.304E-01 (2.274E-02)−	9.383E-01 (4.901E-02)−	3.250E-01 (1.261E-03)
	8	5.923E-01 (3.986E-03)−	5.637E-01 (1.105E-02)−	6.962E-01 (5.020E-02)−	3.587E-01 (4.313E-03)
PMOP10	2	1.543E+00 (1.145E-02)−	2.946E+00 (1.032E+01)−	1.877E+01 (4.407E+02)−	1.168E+00 (2.363E-01)
	3	1.381E+00 (4.538E-02)−	3.758E+00 (2.305E+01)−	2.905E+00 (1.103E+01)−	1.234E+00 (1.360E+00)
	5	1.323E+00 (2.443E-02)−	1.846E+00 (2.594E+00)−	4.728E+00 (1.108E+02)−	1.125E+00 (8.833E-02)
	8	1.112E+00 (3.647E-03)−	2.253E+00 (1.184E+01)−	3.118E+01 (2.060E+03)−	9.489E-01 (8.608E-03)
Sum ('+'/ '−' / '≈')		9/23/0	3/29/0	10/22/0	−

'+', '−' and '≈' indicate that the result is significantly better, significantly worse and statistically similar to that obtained by PD-KI, respectively.

TABLE III
THE KIGD VALUES OF THE CANDIDATE SOLUTION SETS OBTAINED BY KNEE IDENTIFICATION ALGORITHMS FROM THE AUGMENTED SOLUTION SETS ACQUIRED BY KSA TOGETHER WITH THEIR CORRESPONDING INCREMENT VALUES.

Instances	K	Increment	EMU^r	increment	TKR	increment	KnEA	increment	PD-KI
CKP	4	42.56% (4.583E-03)↑	2.437E+00 (3.000E-05)−	-0.02% (0.000E+00)↓	3.853E-01 (5.123E-02)−	87.17% (8.524E-03)↑	6.150E-01 (5.780E-04)−	5.46% (1.105E-02)↑	1.351E-01 (1.009E-03)
	5	8.97% (3.298E-03)↑	2.409E+00 (4.690E-04)−	0.14% (6.500E-05)↑	6.201E-01 (6.441E-02)−	74.92% (1.431E-02)↑	5.960E-01 (7.900E-04)−	1.02% (1.019E-02)↑	1.427E-01 (5.100E-03)
DO2DK	3	2.52% (8.487E-03)↑	1.052E+00 (1.585E-01)−	2.31% (5.274E-03)↑	1.173E+00 (2.580E-01)−	51.51% (2.112E-02)↑	8.584E-01 (1.706E-01)+	2.52% (8.487E-03)↑	9.037E-01 (1.564E-01)
	4	4.12% (1.139E-02)↑	9.202E-01 (1.403E-01)−	7.67% (1.042E-02)↑	1.102E+00 (4.023E-01)−	34.39% (8.056E-02)↑	7.790E-01 (1.548E-01)+	4.71% (1.253E-02)↑	8.113E-01 (1.556E-01)
DEB2DK	4	46.76% (1.899E-02)↑	3.955E-01 (1.212E-02)−	23.78% (6.778E-02)↑	3.060E-01 (2.657E-02)−	90.25% (2.600E-03)↑	3.902E-01 (8.743E-02)−	39.00% (8.624E-02)↑	1.544E-01 (2.968E-03)
	5	12.14% (3.114E-03)↑	7.877E-01 (2.743E-02)−	33.05% (2.645E-02)↑	5.180E-01 (5.598E-03)−	78.88% (1.840E-03)↑	7.414E-01 (1.604E-02)−	0.73% (2.207E-02)↑	2.041E-01 (5.325E-03)
DEB3DK	2	5.74% (1.453E-03)↑	4.244E+00 (2.291E-03)−	-0.03% (0.000E+00)↓	1.745E+00 (7.689E-01)+	30.76% (1.629E-01)↑	1.671E+00 (1.379E+00)+	-7.08% (9.483E-01)↓	1.908E+00 (1.032E+00)
	3	5.30% (1.368E-03)↑	3.943E+00 (6.310E-04)−	-0.05% (3.000E-06)↓	1.784E+00 (3.132E-01)+	11.92% (9.569E-02)↑	1.421E+00 (1.722E+00)+	17.26% (1.615E+00)↑	1.910E+00 (4.182E-01)
Instances	Obj.	Increment	EMU^r	increment	TKR	increment	KnEA	increment	PD-KI
PMOP1	2	19.74% (3.190E-04)↑	8.039E-02 (1.100E-05)−	-0.35% (1.639E-03)↓	8.222E-02 (1.530E-04)−	85.67% (4.660E-04)↑	4.731E-02 (1.000E-06)+	19.74% (3.190E-04)↑	5.233E-02 (8.000E-06)
	3	32.89% (1.260E-03)↑	3.214E-01 (1.045E-03)−	10.67% (7.153E-03)↑	3.088E-01 (2.384E-03)−	56.73% (4.684E-03)↑	1.803E-01 (2.880E-04)+	26.15% (4.832E-03)↑	3.057E-01 (1.998E-03)
	5	22.62% (1.290E-03)↑	1.747E+00 (8.500E-03)−	34.10% (1.396E-03)↑	1.264E+00 (2.015E-02)−	21.68% (3.225E-02)↑	1.631E+00 (5.578E-02)−	-40.47% (4.121E-02)↓	1.033E+00 (4.103E-02)
	8	15.45% (6.733E-03)↑	3.854E+00 (2.467E-01)−	13.52% (5.084E-03)↑	2.815E+00 (1.763E-01)−	-3.45% (6.768E-02)↓	5.274E+00 (4.830E+00)−	25.38% (9.427E-02)↑	2.151E+00 (8.985E-02)
PMOP3	2	10.29% (6.317E-02)↑	8.026E-01 (8.378E-01)+	3.93% (6.440E-02)↑	1.575E+00 (1.547E+00)+	28.33% (1.474E-01)↑	7.621E-01 (8.542E-01)+	2.41% (2.748E-01)↑	1.621E+00 (1.028E+00)
	3	4.63% (1.376E-02)↑	3.230E-01 (5.753E-03)+	5.83% (2.601E-02)↑	9.501E-01 (5.999E-02)−	11.97% (2.611E-02)↑	2.957E-01 (4.896E-03)+	8.12% (4.274E-02)↑	9.267E-01 (5.173E-02)
	5	18.80% (2.225E-02)↑	5.058E-01 (8.568E-03)+	15.84% (2.004E-02)↑	9.212E-01 (1.873E-03)+	-0.55% (2.122E-03)↓	3.964E-01 (6.922E-03)+	21.07% (3.815E-02)↑	2.150E+00 (2.375E-01)
	8	4.30% (4.893E-03)↑	6.687E-01 (7.557E-03)+	6.72% (2.103E-02)↑	9.020E-01 (1.330E-03)+	0.09% (1.139E-03)↑	5.367E-01 (3.412E-03)+	18.92% (3.232E-02)↑	4.942E+00 (1.071E+00)
PMOP4	2	-1.20% (6.116E-03)↓	3.120E+00 (3.278E+00)−	-1.91% (1.222E-02)↓	3.058E+00 (3.261E+00)−	6.18% (2.620E-02)↑	3.077E+00 (3.525E+00)−	-35.26% (1.083E+00)↓	2.936E+00 (3.158E+00)
	3	-6.41% (8.521E-03)↓	4.456E+00 (5.584E+00)+	-6.52% (2.464E-02)↓	4.510E+00 (5.535E+00)+	-2.76% (1.084E-02)↓	4.706E+00 (5.219E+00)−	-8.87% (2.866E-01)↓	4.636E+00 (5.016E+00)
	5	0.67% (4.040E-03)↑	1.209E+00 (3.048E-03)+	2.01% (6.296E-03)↑	2.211E+00 (2.069E-01)−	-9.09% (6.602E-02)↓	1.071E+00 (7.975E-02)+	37.46% (1.441E-01)↑	1.462E+00 (1.210E-01)
	8	-0.23% (1.567E-03)↓	2.771E+00 (5.138E-03)+	2.24% (3.455E-03)↑	5.456E+00 (1.361E+00)+	-2.67% (1.949E-02)↓	2.823E+00 (9.109E-01)+	54.91% (1.365E-01)↑	3.547E+00 (1.535E+00)
PMOP6	2	24.46% (8.785E-01)↑	7.580E-01 (1.494E+00)−	-8.90% (5.657E-01)↓	1.421E+00 (7.419E+00)+	58.85% (3.581E-01)↑	7.286E-01 (1.538E+00)+	24.47% (8.785E-01)↑	7.361E-01 (1.526E+00)
	3	8.33% (9.742E-03)↑	1.738E-01 (5.430E-04)+	8.54% (1.929E-02)↑	4.659E-01 (6.300E-02)−	26.19% (1.715E-01)↑	1.231E-01 (1.016E-03)+	22.09% (9.317E-02)↑	3.330E-01 (2.915E-02)
	5	9.23% (1.334E-02)↑	4.986E-01 (1.469E-02)+	2.49% (4.033E-02)↑	7.188E-01 (1.475E-02)−	3.09% (4.308E-02)↑	3.377E-01 (2.399E-03)+	30.61% (1.110E-01)↑	5.787E-01 (3.037E-02)
	8	17.96% (1.387E-02)↑	1.177E+01 (1.625E-01)−	0.06% (4.880E-04)↑	1.525E+01 (6.785E+00)−	-3.11% (1.870E-02)↓	1.319E+01 (1.342E+01)−	20.20% (4.883E-02)↑	9.572E+00 (1.872E+00)
PMOP7	2	11.59% (1.151E-02)↑	3.669E-01 (1.950E-02)−	48.69% (5.400E-02)↑	2.912E-01 (2.979E-02)−	82.34% (8.470E-03)↑	9.282E-01 (1.648E-02)−	17.95% (2.236E-02)↑	2.464E-01 (2.188E-02)
	3	18.46% (5.048E-03)↑	6.423E-01 (1.925E-02)−	10.76% (2.640E-02)↑	2.821E-01 (2.610E-02)−	62.94% (5.005E-02)↑	7.034E-01 (1.622E-01)−	-20.43% (9.220E-01)↓	2.361E-01 (5.430E-03)
	5	2.36% (4.310E-04)↑	6.157E-01 (2.301E-03)−	1.27% (9.490E-04)↑	3.896E-01 (1.408E-02)−	21.19% (9.282E-02)↑	1.136E+00 (2.486E-01)−	-38.82% (1.216E+00)↓	3.250E-01 (1.261E-03)
	8	1.89% (1.208E-03)↑	5.919E-01 (4.241E-03)−	0.07% (4.080E-04)↑	4.077E-01 (7.016E-03)−	24.93% (5.060E-02)↑	1.977E+00 (7.234E-01)−	-192.34% (1.481E+00)↓	3.587E-01 (4.313E-03)
PMOP10	2	9.30% (1.004E-01)↑	1.417E+00 (8.761E-02)−	7.95% (3.554E-02)↑	3.455E+00 (1.482E+01)−	-14.7% (1.224E+00)↓	7.618E+00 (1.321E+02)−	54.85% (1.107E-01)↑	1.168E+00 (2.363E-01)
	3	2.90% (5.920E-02)↑	1.193E+00 (1.575E-01)+	12.38% (9.630E-02)↑	2.254E+00 (7.716E+00)−	23.55% (1.122E-01)↑	3.114E+00 (1.167E+01)−	-85.77% (1.979E+00)↓	1.234E+00 (1.360E+00)
	5	-1.88% (1.254E-02)↓	1.308E+00 (2.791E-02)−	-0.04% (2.583E-02)↓	3.327E+00 (2.055E+01)−	-70.29% (3.791E+00)↓	8.282E+00 (1.338E+02)−	-151.64% (1.006E+00)↓	1.125E+00 (8.833E-02)
	8	1.85% (1.991E-03)↑	1.115E+00 (3.985E-03)−	-0.28% (1.037E-03)↓	5.544E+00 (6.574E+01)−	-178.89% (2.301E+01)↓	3.719E+01 (2.052E+03)−	-46.87% (1.515E+00)↓	9.489E-01 (8.608E-03)
sum('+'/'−' /'≈')		−	10/22/0	−	8/24/0	−	15/17/0	−	−
Sum ('↑' / '↓')		28/4	−	23/9	−	23/9	−	20/10	−

'+', '−' and '≈' indicate that the result is significantly better, significantly worse and statistically similar to that obtained by PD-KI, respectively. '↑' (or '↓') indicates that the increment is positive or negative.

regions, the increment values become negative. The results investigating the influences of the distribution of the solutions and the limitations of KSA are presented in Section II and Section III of the Supplementary material, respectively.

In summary, the results in Tables II and III show that PD-KI outperforms the compared methods in identifying knee regions on most instances, and KSA is able to improve the performance of knee identification algorithms in the search of knee solutions according to the KIGD and the increment values.

2) Analysis of KD results: In this section, an analysis of the KD results presented in Table IV and Table V is given.

Table IV presents the KD values of all methods. According to the best values, PD-KI performs the best with 20 best records, followed by EMU^r with 10 best records out of 32 instances. According to the rank sum values, PD-KI outperforms others in identifying knee solutions on most instances. Specifically, PD-KI wins on 22, 30, and 26 out of 32 instances in comparison with EMU^r, TKR, and KnEA, respectively. The better performance of PD-KI can be attributed to the solution set augmented by KSA. Overall, PD-KI outperforms others on most instances according to the KD values.

Table V presents the KD values and corresponding increment values obtained by the identification methods based on the augmented solution set provided by KSA. The increment values in the first column show that KSA is able to generate promising candidates close to the true knee points on most instances because there are 26 wins against 6 losses. The results also show that the performances of the identification methods under comparison have also improved on most instances. For example, the performances of EMU^r, TKR, and KnEA are enhanced on 21, 22, and 19 instances in terms of the sum of $\uparrow$, respectively. According to the rank sum values, the performances of KnEA and EMU^r are greatly improved, since both have obtained 13 better results than PD-KI. Especially, KnEA achieves the best result on 13 instances while PD-KI achieves the best results on 15 instances. Therefore, KSA is also able to improve the performance of existing methods in search for knee solutions. However, some increment values in Table V are negative. This happens mainly on problems such as PMOP4, which is hard for an EA to converge due to its strong multimodality and complicated asymmetry of its PoF. Since the solutions are poorly converged, KSA may fail to produce promising solutions in the knee regions.

In summary, the results in Tables IV and V confirm that PD-KI is competitive in identifying knee regions on most test instances, and KSA is able to enhance the performance of knee identification algorithms in terms of KD and the increment values. More analyses on KSA are presented in Sections V and VII of the Supplementary material.

D. Results on hybrid electric vehicle controller management

1) Problem description: Here, we apply the proposed method to a hybrid electric vehicle (HEV) management controller design problem [62]. Fig. 6 illustrates the general architecture of HEV controller management system. Especially, the controller provides the vehicles with the propulsion

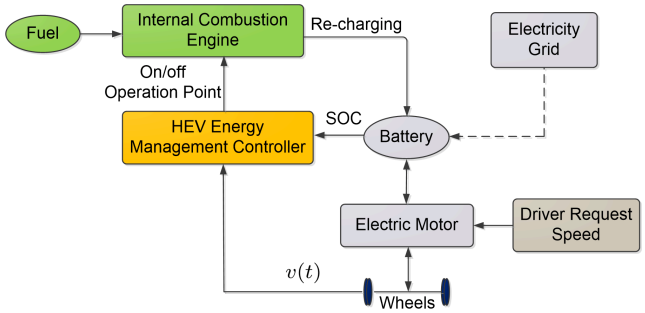

Fig. 6. The general architecture of the HEV, where the fuel and battery are the power sources to the internal combustion engine (ICE) and electric motor (EM), respectively; the battery can be charged from the electricity grids or recharged during the braking; the request speed from the driver determines the torque generated by the electric motor; the HEV energy management controller controls the internal combustion engine by switching the operation point in terms of the state-of-change (SOC) and current speed $v(t)$.

by a combination of an internal combustion engine (ICE) and an electric motor (EM), and the energy management controller is required to maximize the required performance by switching the power sources between the ICE and EM during different driving scenarios [63]. The HEV controller operates by tuning 11 parameters under a set of rules to minimize seven objectives, i.e., the fuel consumption (FC), battery stress (BS), operation changes (OC), emission, noise, urban operation (UO), and battery state of change (SOC). The interested readers are referred to [62] for more details of the hybrid electric vehicle management controller design problem.

2) Knee-oriented augmentation on HEV controller management: In order to test the performance of KSA, a solution set with 66 non-dominated solutions is obtained by RVEA [62] on the HEV controller design problem, as shown in Fig. 7 (a). Fig. 7 (b) plots the augmented results with 83 non-dominated solutions (under the condition of 200 fitness evaluations). The normalized hypervolume (HV) [64] values of the solution sets in Figs. 7 (a) and (b) are 7.81E-3 and 7.94E-3, respectively. With data augmentation by KSA, the performance is improved by 1.67% in terms of the HV value, indicating that KSA is able to improve the quality of the solution set.

3) Proposed measurement for knee verification: Here we examine whether the knee solutions obtained by four knee identification methods on the basis of the solution set plotted in Figs. 7 (a) and (b) are really knee solutions.

To the best of our knowledge, no measure has been proposed for the verification of the knee candidates when the PoF of the problem is unknown. Accordingly, a verification method assisted by the boxplot is introduced to further investigate the acquired solutions whether they are true knee candidates or not. According to the definition of the knee point in Eq. 2, the knee points are the solutions with largest distances to the hyperplane, in comparison with their neighboring solutions. In this study, the number of solutions in the neighborhood of each obtained solution is set to 5, 10, and 15. Taking Fig. 9 as an example, the y-axis value closer to 5, 10, and 15 means that the obtained knee candidates have larger distance to the hyperplane than their 5, 10, and 15 neighboring solutions. In other words, the solutions from the obtained solution set are

TABLE IV
THE KD VALUES OF THE CANDIDATE SOLUTION SETS OBTAINED BY THE IDENTIFICATION METHODS.

Instances	K	EMU^r	TKR	KnEA	PD-KI
CKP	4	2.255E+00 (2.700E-05)−	3.226E+00 (2.590E-01)−	7.684E-01 (7.111E-03)−	1.281E-01 (2.133E-03)
	5	2.236E+00 (2.500E-05)−	2.700E+00 (7.257E-01)−	5.618E-01 (4.137E-03)−	1.313E-01 (4.895E-03)
DO2DK	3	1.150E+00 (2.152E-01)−	2.656E+00 (7.618E-01)−	9.262E-01 (1.589E-01)−	9.636E-01 (1.725E-01)
	4	1.066E+00 (1.294E-01)−	1.881E+00 (9.395E-02)−	8.557E-01 (1.672E-01)+	8.599E-01 (1.693E-01)
DEB2DK	4	5.510E-01 (1.175E-01)−	3.134E+00 (2.070E-03)−	6.295E-01 (1.343E-01)−	1.283E-01 (3.685E-03)
	5	1.149E+00 (5.292E-02)−	2.468E+00 (2.763E-01)−	7.565E-01 (1.917E-02)−	1.592E-01 (8.890E-03)
DEB3DK	2	4.109E+00 (2.477E-03)−	2.955E+00 (6.847E-01)−	2.257E+00 (1.553E+00)−	2.119E+00 (1.148E+00)
	3	3.673E+00 (5.700E-04)−	2.376E+00 (7.200E-01)−	2.999E+00 (2.821E+00)−	1.992E+00 (4.540E-01)
Instances	Obj.	EMU^r	TKR	KnEA	PD-KI
PMOP1	2	8.436E-02 (0.000E+00)−	5.612E-01 (0.000E+00)−	8.436E-02 (0.000E+00)−	7.009E-02 (1.800E-05)
	3	2.727E-01 (0.000E+00)−	7.030E-01 (0.000E+00)−	2.727E-01 (0.000E+00)−	2.517E-01 (4.626E-03)
	5	2.675E+00 (2.418E-02)−	1.501E+00 (7.554E-02)−	9.060E-01 (5.000E-06)−	1.028E+00 (1.647E-02)
	8	4.714E+00 (3.004E-01)−	2.516E+00 (9.321E-01)−	6.980E+00 (2.223E+00)−	2.351E+00 (1.145E-01)
PMOP3	2	7.762E-01 (7.611E-01)+	2.323E+00 (1.882E+00)−	8.204E-01 (7.794E-01)+	1.084E+00 (9.416E-01)
	3	2.805E-01 (1.147E-02)+	1.064E+00 (3.556E-02)−	2.938E-01 (1.335E-02)+	8.159E-01 (1.061E-01)
	5	6.918E-01 (5.486E-03)−	9.501E-01 (1.468E-03)−	5.456E-01 (1.531E-02)+	6.106E-01 (5.044E-02)
	8	7.656E-01 (4.171E-03)+	9.400E-01 (1.656E-03)−	8.127E-01 (2.698E-01)+	8.228E-01 (1.154E-02)
PMOP4	2	2.996E+00 (2.809E+00)−	3.160E+00 (3.218E+00)−	1.844E+01 (4.971E+03)−	2.945E+00 (3.205E+00)
	3	4.356E+00 (5.932E+00)+	4.441E+00 (5.440E+00)+	3.848E+01 (8.939E+03)−	4.680E+00 (5.038E+00)
	5	1.226E+00 (1.043E-02)+	1.958E+00 (2.082E-01)+	1.295E+01 (2.443E+03)−	1.475E+00 (8.058E-02)
	8	2.753E+00 (2.832E-02)+	4.853E+00 (1.330E+00)−	3.802E+01 (9.936E+03)−	3.348E+00 (1.152E+00)
PMOP6	2	6.829E-01 (1.361E+00)+	2.272E+00 (4.672E+00)−	6.931E-01 (1.361E+00)+	7.402E-01 (1.580E+00)
	3	1.545E-01 (5.296E-03)+	6.537E-01 (4.399E-02)−	2.760E-01 (1.021E-01)−	2.612E-01 (3.526E-02)
	5	3.131E-01 (3.093E-02)+	5.452E-01 (1.759E-02)−	7.161E-01 (6.341E-01)−	4.002E-01 (4.253E-02)
	8	9.209E-01 (2.044E-01)+	3.216E+00 (8.191E+00)−	8.824E+00 (9.946E+01)−	1.634E+00 (3.363E-01)
PMOP7	2	8.175E-01 (2.441E-01)−	1.627E+00 (9.665E-02)−	1.227E+00 (1.255E-01)−	2.281E-01 (2.504E-02)
	3	6.863E-01 (1.540E-02)−	8.237E-01 (9.087E-03)−	6.937E-01 (8.446E-02)−	1.959E-01 (6.229E-03)
	5	5.608E-01 (2.396E-03)−	5.286E-01 (3.729E-02)−	9.987E-01 (5.524E-02)−	2.967E-01 (2.190E-03)
	8	5.452E-01 (5.577E-03)−	5.107E-01 (1.118E-02)−	7.233E-01 (5.313E-02)−	3.239E-01 (6.819E-03)
PMOP10	2	1.543E+00 (1.100E-02)−	2.946E+00 (1.033E+01)−	1.878E+01 (4.407E+02)−	1.171E+00 (2.316E-01)
	3	1.376E+00 (4.486E-02)−	3.755E+00 (2.307E+01)−	2.917E+00 (1.095E+01)−	1.241E+00 (1.360E+00)
	5	1.323E+00 (1.635E-02)−	1.787E+00 (2.618E+00)−	4.704E+00 (1.117E+02)−	1.122E+00 (8.908E-02)
	8	1.163E+00 (1.239E-02)−	2.244E+00 (1.185E+01)−	3.113E+01 (2.059E+03)−	9.852E-01 (4.654E-03)
Sum ('+'/ '−' / '≈')		10/22/0	2/30/0	6/26/0	–

'+', '−' and '≈' indicate that the result is significantly better, significantly worse and statistically similar to that obtained by PD-KI, respectively.

TABLE V
THE KD VALUES OF THE CANDIDATE SOLUTION SETS OBTAINED BY THE IDENTIFICATION METHODS IN TERMS OF THE AUGMENTED SOLUTION SET ACQUIRED BY KSA, AND THEIR CORRESPONDING INCREMENT VALUES.

Instances	K	Increment	EMU^r	increment	TKR	increment	KnEA	increment	PD-KI
CKP	4	49.42% (3.600E-02)↑	2.256E+00 (3.200E-05) −	-0.02% (0.000E+00)↓	4.053E-01 (4.909E-02)−	86.92% (6.375E-03)↑	7.118E-01 (8.800E-04)−	6.11% (1.583E-02)↑	1.281E-01 (2.133E-03)
	5	38.50% (6.295E-02)↑	2.233E+00 (3.040E-04)−	0.12% (4.600E-05)↑	5.461E-01 (6.961E-02) −	78.21% (1.245E-02)↑	5.129E-01 (1.806E-03)−	7.80% (1.179E-02)↑	1.313E-01 (4.895E-03)
DO2DK	3	1.91% (7.845E-03)↑	1.130E+00 (2.105E-01) −	1.72% (4.087E-03)↑	1.224E+00 (3.018E-01) −	54.41% (2.464E-02)↑	9.237E-01 (1.797E-01)+	1.91% (7.845E-03)↑	9.636E-01 (1.725E-01)
	4	4.61% (1.508E-02)↑	9.882E-01 (1.610E-01)−	9.88% (2.202E-02)↑	1.157E+00 (4.638E-01)−	40.28% (7.685E-02)↑	8.221E-01 (1.626E-01)+	5.44% (1.782E-02)↑	8.599E-01 (1.693E-01)
DEB2DK	4	30.48% (3.710E-02)↑	3.076E-01 (1.983E-02)−	29.18% (9.385E-02)↑	2.528E-01 (3.848E-02)−	91.98% (3.782E-03)↑	3.920E-01 (1.244E-01)−	38.83% (1.374E-01)↑	1.283E-01 (3.685E-03)
	5	44.59% (3.708E-02)↑	4.654E-01 (8.223E-02)−	60.09% (4.784E-02)↑	2.538E-01 (1.430E-02)−	89.34% (2.973E-03)↑	7.381E-01 (2.248E-02)−	-0.48% (5.817E-02)↓	1.592E-01 (8.890E-03)
DEB3DK	2	0.29% (9.910E-04)↑	4.110E+00 (2.533E-03)−	-0.03% (0.000E+00)↓	1.896E+00 (9.010E-01)+	29.19% (1.807E-01)↑	1.873E+00 (1.279E+00)+	-3.05% (6.625E-01)↓	2.119E+00 (1.148E+00)
	3	5.13% (2.207E-03)↑	3.676E+00 (6.630E-04)−	-0.07% (4.000E-06)↓	1.927E+00 (4.215E-01)≈	10.77% (1.426E-01)↑	1.536E+00 (1.833E+00)+	15.53% (1.345E+00)↑	1.992E+00 (4.540E-01)
Instances	Obj.	Increment	EMU^r	increment	TKR	increment	KnEA	increment	PD-KI
PMOP1	2	18.52% (1.548E-03)↑	6.874E-02 (1.100E-05)+	18.52% (1.548E-03)↑	7.921E-02 (1.770E-04)−	85.88% (5.630E-04)↑	6.874E-02 (1.100E-05)+	18.52% (1.548E-03)↑	7.009E-02 (1.800E-05)
	3	29.54% (6.448E-03)↑	2.126E-01 (1.104E-03)+	22.04% (1.486E-02)↑	2.668E-01 (3.576E-03)−	62.04% (7.241E-03)↑	1.927E-01 (5.200E-04)+	29.31% (7.003E-03)↑	2.517E-01 (4.626E-03)
	5	15.60% (2.662E-03)↑	1.757E+00 (9.045E-03)−	34.14% (2.083E-03)↑	1.191E+00 (4.055E-02)−	16.84% (7.800E-02)↑	1.411E+00 (3.940E-02)−	-55.68% (4.753E-02)↓	1.028E+00 (1.647E-02)
	8	8.06% (1.778E-03)↑	3.859E+00 (1.213E-01)−	17.49% (7.438E-03)↑	2.737E+00 (3.305E-01)−	-18.68% (1.503E-01)↓	5.074E+00 (4.653E+00)−	25.68% (9.360E-02)↑	2.351E+00 (1.145E-01)
PMOP3	2	-1.57% (1.490E-01)↓	8.046E-01 (8.534E-01)+	-4.08% (1.262E-01)↓	1.645E+00 (1.663E+00)−	29.53% (1.438E-01)↑	7.823E-01 (8.505E-01)+	-5.64% (3.932E-01)↓	1.084E+00 (9.416E-01)
	3	-4.46% (3.198E-02)↓	2.763E-01 (8.833E-03)+	-2.24% (4.711E-02)↓	9.303E-01 (6.354E-02)−	12.72% (2.721E-02)↑	2.751E-01 (5.727E-03)+	-0.53% (7.353E-02)↓	8.159E-01 (1.061E-01)
	5	26.10% (5.341E-02)↑	5.452E-01 (1.858E-02)+	20.50% (4.185E-02)↑	9.537E-01 (2.074E-03)−	-0.44% (2.031E-03)↓	4.208E-01 (1.390E-02)+	21.21% (5.470E-02)↑	6.106E-01 (5.044E-02)
	8	5.04% (1.067E-02)↑	7.131E-01 (8.492E-03)+	6.48% (1.576E-02)↑	9.389E-01 (1.512E-03)−	0.06% (1.114E-03)↑	6.400E-01 (2.009E-03)+	11.61% (2.879E-02)↑	8.228E-01 (1.154E-02)
PMOP4	2	0.61% (2.150E-02)↑	3.133E+00 (3.293E+00)−	-2.04% (1.189E-02)↓	3.067E+00 (3.274E+00)−	6.29% (3.211E-02)↑	3.089E+00 (3.545E+00)−	-36.35% (1.317E+00)↓	2.945E+00 (3.205E+00)
	3	-6.90% (1.192E-02)↓	4.494E+00 (5.653E+00)+	-6.48% (2.467E-02)↓	4.513E+00 (5.538E+00)+	-2.31% (1.036E-02)↓	4.752E+00 (5.240E+00)−	-9.43% (2.770E-01)↓	4.680E+00 (5.038E+00)
	5	0.93% (3.156E-03)↑	1.202E+00 (5.971E-03)+	1.54% (5.552E-03)↑	2.072E+00 (1.708E-01)−	-8.66% (5.931E-02)↓	1.104E+00 (6.732E-02)+	34.18% (1.470E-01)↑	1.475E+00 (8.058E-02)
	8	-1.25% (1.828E-03)↓	2.676E+00 (9.252E-03)+	2.53% (3.047E-03)↑	4.928E+00 (1.058E+00)−	-3.37% (2.641E-02)↓	2.739E+00 (8.394E-01)+	53.00% (1.357E-01)↑	3.348E+00 (1.152E+00)
PMOP6	2	16.22% (1.689E+00)↑	7.402E-01 (1.580E+00)≈	16.22% (1.689E+00)↑	1.397E+00 (7.588E+00)−	63.12% (3.664E-01)↑	7.402E-01 (1.580E+00)≈	16.22% (1.689E+00)↑	7.402E-01 (1.580E+00)
	3	1.97% (9.550E-04)↑	1.445E-01 (4.865E-03)+	5.62% (1.168E-02)↑	4.138E-01 (8.629E-02) −	33.43% (2.174E-01)↑	1.382E-01 (4.624E-03)+	15.26% (1.100E-01)↑	2.612E-01 (3.526E-02)
	5	0.63% (2.533E-03)↑	3.816E-01 (5.652E-02)+	-40.37% (1.447E+00)↓	5.368E-01 (2.241E-02) −	-3.90% (1.372E-01)↓	2.645E-01 (8.495E-03)+	24.55% (1.489E-01)↑	4.002E-01 (4.253E-02)
	8	-0.15% (1.416E-02)↓	9.333E-01 (2.303E-01)+	-1.46% (2.626E-02)↓	3.905E+00 (1.711E+01) −	-55.51% (1.868E+00)↓	2.648E+00 (2.355E+01)−	5.26% (1.865E+00)↑	1.634E+00 (3.363E-01)
PMOP7	2	10.31% (2.239E-02)↑	2.689E-01 (2.972E-02)−	58.66% (5.926E-02)↑	2.839E-01 (3.628E-02)−	82.94% (1.005E-02)↑	1.006E+00 (1.276E-02)−	14.65% (2.292E-02)↑	2.281E-01 (2.504E-02)
	3	2.76% (2.751E-03)↑	6.014E-01 (2.136E-02)−	11.55% (2.997E-02)↑	2.922E-01 (3.239E-02)−	63.96% (5.349E-02)↑	7.321E-01 (1.606E-01)−	-20.62% (9.030E-01)↓	1.959E-01 (6.229E-03)
	5	0.72% (5.310E-04)↑	5.557E-01 (2.248E-03)−	0.86% (5.850E-04)↑	4.025E-01 (1.958E-02)−	13.86% (1.782E-01)↑	1.196E+00 (2.400E-01)−	-36.62% (1.043E+00)↓	2.967E-01 (2.190E-03)
	8	1.48% (2.346E-03)↑	5.440E-01 (5.720E-03)−	0.22% (2.650E-04)↑	3.861E-01 (1.108E-02)−	21.72% (6.385E-02)↑	2.011E+00 (7.242E-01)−	-186.65% (1.388E+00)↓	3.239E-01 (6.819E-03)
PMOP10	2	9.44% (9.398E-02)↑	1.424E+00 (8.061E-02)−	7.39% (3.427E-02)↑	3.457E+00 (1.483E+01)−	-14.78% (2.143E-01)↓	7.617E+00 (1.322E+02)−	55.00% (1.101E-01)↑	1.171E+00 (2.316E-01)
	3	3.33% (6.176E-02)↑	1.181E+00 (1.574E-01)+	12.88% (9.891E-02)↑	2.245E+00 (7.691E+00)−	23.66% (1.091E-01)↑	3.104E+00 (1.169E+01)−	-80.54% (1.922E+00)↓	1.241E+00 (1.360E+00)
	5	-0.10% (1.151E-02)↓	1.317E+00 (2.945E-02)−	-0.37% (2.442E-02)↓	3.276E+00 (2.089E+01)−	-71.08% (4.026E+00)↓	8.175E+00 (1.343E+02)−	-163.53% (1.522E+00)↓	1.122E+00 (8.908E-02)
	8	1.47% (1.667E-03)↑	1.170E+00 (1.156E-02)−	-0.68% (9.180E-04)↓	5.572E+00 (6.554E+01)−	-189.74% (2.545E+01)↓	3.710E+01 (2.054E+03)−	-45.45% (1.554E+00)↓	9.852E-01 (4.654E-03)
Sum ('+'/'−'/ '≈')		–	13/18/1	–	2/29/1	–	14/17/1	–	–
Sum ('↑' / '↓')		26/6	–	21/11	–	22/10	–	19/13	–

'+', '−' and '≈' indicate that the result is significantly better, significantly worse and statistically similar to that obtained by PD-KI, respectively. '↑' (or '↓') indicates that the increment is positive or negative.

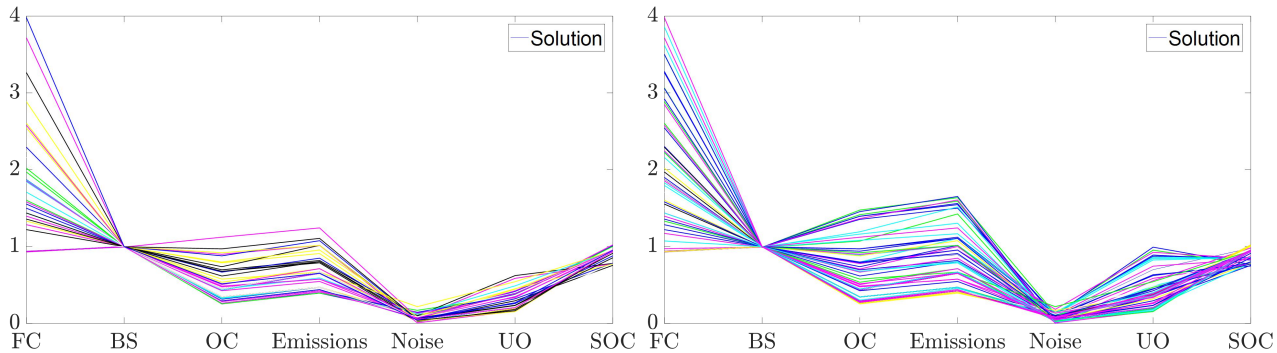

(a) Before (b) After

Fig. 7. (a) The solution set obtained by RVEA before the augmentation by KSA. (b) The solution set augmented by KSA. The lines are denoted by the solutions.

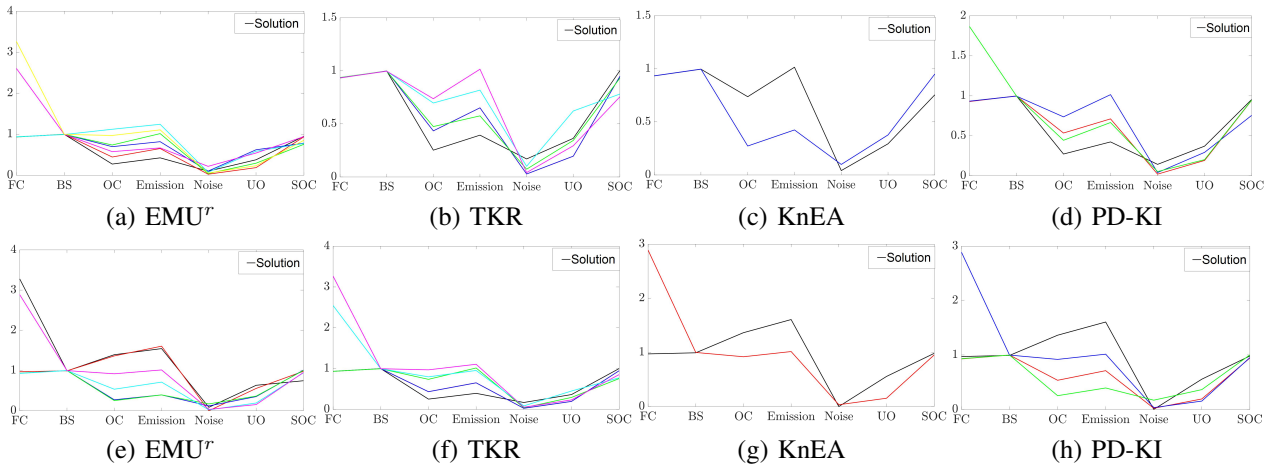

(a) EMU^r (b) TKR (c) KnEA (d) PD-KI

(e) EMU^r (f) TKR (g) KnEA (h) PD-KI

Fig. 8. Plots (a) - (d) show the knee candidates obtained by EMU^r, TKR, KnEA, and PD-KI on Fig. 7 (a). Plots (e) - (h) present the knee candidates obtained by the four methods on Fig. 7 (b).

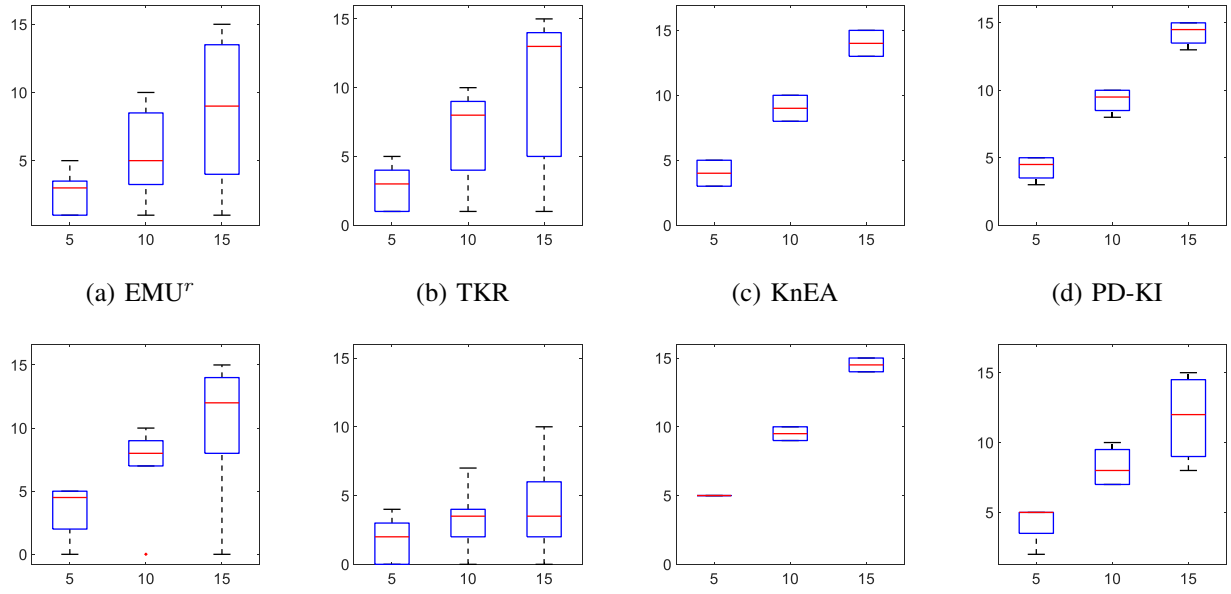

(a) EMU^r (b) TKR (c) KnEA (d) PD-KI

(e) EMU^r (f) TKR (g) KnEA (h) PD-KI

Fig. 9. Plots (a) - (d) show the boxplots of the knee candidates obtained by EMU^r, TKR, KnEA, and PD-KI, respectively, where all results are based on Fig. 7 (a). Plots (e) - (h) present the boxplots of knee candidates acquired by the four methods in terms of Fig. 7 (b). The x-axis represents the number of solutions in the neighborhood (5, 10, and 15). The y-axis shows the number of solutions whose distances to the hyperplane are smaller than that of the achieved solutions.

more likely to be the true knee solutions. On the contrary, the value closer to 0 denotes that the solutions from the solution set may be isolated or close to the boundary because they are closer to the hyperplane.

The solutions obtained by the compared algorithms shown in Fig. 8 are replotted in Fig. 9 using boxplots. Specifically, the results in Figs. 9 (a) - (d) are based on the solution set without augmentation (Fig. 7 (a)), while those in Figs. 9 (e) - (h) are based on the augmented solution set (Fig. 7 (b)). From Figs. 9 (a) - (d), we observe PD-KI and KnEA show better performance, because their median values of the boxplots are larger than that of other methods. This means the provided solutions are more likely the true knee candidates. However, PD-KI identifies more diverse knee candidates than KnEA, as shown in Figs. 8 (c) and (d). Figs. 9 (a) - (d) also show that all methods have found at least one true knee candidate of the solution set, because the maximum y-axis value of the boxplot is 5, 10, and 15. However, Figs. 9 (a) and (b) also contain isolated solutions whose y-axis value is approximately 0, because these two methods favor the boundary points during the selection.

Figs. 9 (e) - (h) show that KnEA has the best performance with the largest median value, followed by PD-KI and EMU^r. But PD-KI and EMU^r provide more diverse knee candidates than KnEA. PD-KI, KnEA and EMU^r have found the true knee candidates of the augmented solution set, while TKR did not find any true knee solutions since the maximum y-axis value is not equal to 5, 10, and 15. Notably, EMU^r and

TKR also identify isolated solutions or boundary solutions, whose minimum y-axis value equals 0, 0, and 0 on different x-labels (5, 10, and 15), respectively.

In summary, the results on the HEV controller design problem demonstrate that KSA is able to enhance the quality of the solution set, and PD-KI is effective in the search for diverse knee solutions and able to provide promising knee candidates rather than the isolated solutions or boundary points.

V. Conclusion

Identification of knee points from a set of approximated solutions is non-trivial if no sufficient solutions are available around the knee points, in particular when the number of objectives becomes large.

To address the above challenge, this paper proposes a framework that augments the given solution set for knee identifications by generating promising solutions in the knee regions. By transforming the non-dominated front into a multimodal auxiliary function and building an inverse model, the proposed knee-oriented solution augmentation algorithm is able to generate well distributed solutions around the potential knee points, thereby making it much easier for a knee identification algorithm to more effectively detect the knee points. For verification of knee solutions without the knowledge of the true Pareto front, this paper also proposes a boxplot assisted method for the verification of knee candidates. A set of experiments is conducted on 32 benchmark problems and on a hybrid electric vehicle controller design problem. The experimental results demonstrate that the proposed solution augmentation method is effective in enhancing the quality of the identified knee points of all knee identification algorithms investigated in this study.

One topic of future research is to improve the effectiveness in generating high-quality solutions when the knee regions are complex, especially in a high-dimensional objective space. Another interesting yet challenging topic is to develop new methods that can more effectively deal with multiobjective optimization problems having many local Pareto fronts. Finally, inverse modeling will become increasingly hard when the number of decision variables becomes large. In this case, random grouping or other dimension reduction methods may be helpful.

Acknowledgment

This work was supported in part by the Honda Research Institute Europe GmbH, and funded by National Natural Science Foundation of China (No. 62103150, and 62136003), the China Postdoctoral Science Foundation (No. 2021M691012), the Key Project of Science and Technology Innovation 2030 Supported by the Ministry of Science and Technology of China (No. 2018AAA0101302), National Natural Science Foundation of China (Basic Science Center Program: No. 61988101), National Natural Science Fund for Distinguished Young Scholars (No. 61725301), and International (Regional) Cooperation and Exchange Project (No. 61720106008). YJ is supported in part by an Alexander von Humboldt Professor for Artificial Intelligence endowed by the German Federal Ministry of Education and Research.

References

[1] K. Miettinen, *Nonlinear multiobjective optimization*. Springer Science & Business Media, 2012.

[2] A. Zhou, B.-Y. Qu, H. Li, S.-Z. Zhao, P. N. Suganthan, and Q. Zhang, "Multiobjective evolutionary algorithms: A survey of the state of the art," *Swarm and Evolutionary Computation*, vol. 1, no. 1, pp. 32–49, 2011.

[3] B. Li, J. Li, K. Tang, and X. Yao, "Many-objective evolutionary algorithms: A survey," *ACM Computing Surveys (CSUR)*, vol. 48, no. 1, pp. 1–35, 2015.

[4] L. Ma, M. Huang, S. Yang, R. Wang, and X. Wang, "An adaptive localized decision variable analysis approach to large-scale multiobjective and many-objective optimization," *IEEE Transactions on Cybernetics*, pp. 1–13, 2021.

[5] G. Yu, R. Shen, J. Zheng, M. Li, J. Zou, and Y. Liu, "Binary search based boundary elimination selection in many-objective evolutionary optimization," *Applied Soft Computing*, vol. 60, pp. 689 – 705, 2017.

[6] G. Yu, J. Zheng, R. Shen, and M. Li, "Decomposing the user-preference in multiobjective optimization," *Soft Computing*, vol. 20, no. 10, pp. 4005–4021, 2016.

[7] M. Velasquez and P. T. Hester, "An analysis of multi-criteria decision making methods," *International Journal of Operations Research*, vol. 10, no. 2, pp. 56–66, 2013.

[8] R. C. Purshouse, K. Deb, M. M. Mansor, S. Mostaghim, and R. Wang, "A review of hybrid evolutionary multiple criteria decision making methods," in *Proceedings of the 2000 Congress on Evolutionary Computation*. IEEE, 2014, pp. 1147–1154.

[9] H. Wang, M. Olhofer, and Y. Jin, "A mini-review on preference modeling and articulation in multi-objective optimization: current status and challenges," *Complex & Intelligent Systems*, vol. 3, no. 4, pp. 233–245, 2017.

[10] G. Yu, Y. Jin, and M. Olhofer, "References or preferences–rethinking many-objective evolutionary optimization," in *2019 IEEE Congress on Evolutionary Computation (CEC)*. IEEE, 2019, pp. 2410–2417.

[11] B. Jürgen, D. Kalyanmoy, D. Henning, and O. Matthias, "Finding knees in multi-objective optimization," in *Proceedings of the International Conference on Parallel Problem Solving from Nature*, vol. 3242. Berlin, Heidelberg: Springer, 2004, pp. 722–731.

[12] X. Zhang, Y. Tian, and Y. Jin, "A knee point-driven evolutionary algorithm for many-objective optimization," *IEEE Transactions on Evolutionary Computation*, vol. 19, no. 6, pp. 761–776, 2015.

[13] T. Chen, K. Li, R. Bahsoon, and X. Yao, "FEMOSAA: Feature-guided and knee-driven multi-objective optimization for self-adaptive software," *ACM Transactions on Software Engineering and Methodology (TOSEM)*, vol. 27, no. 2, pp. 1–50, 2018.

[14] M. Jiang, Z. Wang, H. Hong, and G. G. Yen, "Knee point-based imbalanced transfer learning for dynamic multiobjective optimization," *IEEE Transactions on Evolutionary Computation*, vol. 25, no. 1, pp. 117–129, 2021.

[15] J. Zou, Q. Li, S. Yang, H. Bai, and J. Zheng, "A prediction strategy based on center points and knee points for evolutionary dynamic multi-objective optimization," *Applied Soft Computing*, vol. 61, pp. 806–818, 2017.

[16] S. M. Alzahrani and N. Wattanapongsakorn, "Comparative study of knee-based algorithms for many-objective optimization problems," *Transactions on Computer and Information Technology (ECTI-CIT)*, vol. 12, no. 1, pp. 7–16, 2018.

[17] C. Yue, J. Liang, B. Qu, H. Song, G. Li, and Y. Han, "A knee point driven particle swarm optimization algorithm for sparse reconstruction," in *Asia-Pacific Conference on Simulated Evolution and Learning*. Springer, 2017, pp. 911–919.

[18] A. K. Nandi, D. Chakraborty, and W. Vaz, "Design of a comfortable optimal driving strategy for electric vehicles using multi-objective optimization," *Journal of Power Sources*, vol. 283, pp. 1–18, 2015.

[19] Y. Zhou, G. G. Yen, and Z. Yi, "A knee-guided evolutionary algorithm for compressing deep neural networks," *IEEE Transactions on Cybernetics*, vol. 51, no. 3, pp. 1626–1638, 2021.

[20] J. Luo, L. Jiao, F. Liu, S. Yang, and W. Ma, "A Pareto-based sparse subspace learning framework," *IEEE Transactions on Cybernetics*, vol. 49, no. 11, pp. 3859–3872, 2019.

[21] Z. Li, J. Liu, and K. Wu, "A multiobjective evolutionary algorithm based on structural and attribute similarities for community detection in attributed networks," *IEEE Transactions on Cybernetics*, vol. 48, no. 7, pp. 1963–1976, 2018.

[22] K. Deb and S. Gupta, "Understanding knee points in bicriteria problems and their implications as preferred solution principles," *Engineering Optimization*, vol. 43, no. 11, pp. 1175–1204, 2011.

[23] B. Marlon, S. Pradyumn, and S. Hartmut, "Angle-based preference models in multi-objective optimization," in *Proceedings of the International Conference on Evolutionary Multi-Criterion Optimization*. Springer, February 2017, pp. 88–102.

[24] S. Sufian and W. Naruemon, "Adaptive geometric angle-based algorithm with independent objective biasing for pruning Pareto-optimal solutions," in *Proceedings of the 2013 Science and Information Conference*. London, UK: IEEE, October 2013, pp. 514–523.

[25] I. Das, "On characterizing the knee of the Pareto curve based on normal-boundary intersection," *Structural Optimization*, vol. 18, no. 2-3, pp. 107–115, 1999.

[26] S. Oliver, L. Marco, and C. C. A. Coello, "Approximating the knee of an mop with stochastic search algorithms," in *International Conference on Parallel Problem Solving from Nature*. Springer, 2008, pp. 795–804.

[27] K. Bhattacharjee, H. Singh, M. Ryan, and T. Ray, "Bridging the gap: Many-objective optimization and informed decision-making," *IEEE Transactions on Evolutionary Computation*, vol. 21, no. 5, pp. 813–820, 2017.

[28] G. Yu, Y. Jin, and M. Olhofer, "An a priori knee identification multi-objective evolutionary algorithm based on α-dominance," in *Proceedings of the Genetic and Evolutionary Computation Conference Companion*, ser. GECCO'19. New York, NY, USA: Association for Computing Machinery, 2019, pp. 241–242.

[29] ——, "A multiobjective evolutionary algorithm for finding knee regions using two localized dominance relationships," *IEEE Transactions on Evolutionary Computation*, vol. 25, no. 1, pp. 145–158, 2021.

[30] B. Slim, S. L. Ben, and K. Ghédira, "Searching for knee regions of the Pareto front using mobile reference points," *Soft Computing*, vol. 15, no. 9, pp. 1807–1823, 2011.

[31] L. Rachmawati and D. Srinivasan, "Multiobjective evolutionary algorithm with controllable focus on the knees of the Pareto front," *IEEE Transactions on Evolutionary Computation*, vol. 13, no. 4, pp. 810–824, 2009.

[32] K. Zhang, G. G. Yen, and Z. He, "Evolutionary algorithm for knee-based multiple criteria decision making," *IEEE Transactions on Cybernetics*, vol. 51, no. 2, pp. 722–735, 2021.

[33] G. Yu, Y. Jin, and M. Olhofer, "A method for *a posteriori* identification of knee points based on solution density," in *Proceedings of the 2018 IEEE Congress on Evolutionary Computation (CEC)*. Rio de Janeiro, Brazil: IEEE, 2018, pp. 1–8.

[34] S. Sudeng and N. Wattanapongsakorn, "A decomposition-based approach for knee solution approximation in multi-objective optimization," in *Proceedings of the 2016 IEEE Congress on Evolutionary Computation (CEC)*. IEEE, 2016, pp. 3710–3717.

[35] Y. Jin, "Surrogate-assisted evolutionary computation: Recent advances and future challenges," *Swarm and Evolutionary Computation*, vol. 1, no. 2, pp. 61–70, 2011.

[36] T. Chugh, K. Sindhya, J. Hakanen, and K. Miettinen, "A survey on handling computationally expensive multiobjective optimization problems with evolutionary algorithms," *Soft Computing*, vol. 23, no. 9, pp. 3137–3166, 2019.

[37] Y. Jin, H. Wang, T. Chugh, D. Guo, and K. Miettinen, "Data-driven evolutionary optimization: An overview and case studies," *IEEE Transactions on Evolutionary Computation*, vol. 23, no. 3, pp. 442–458, 2019.

[38] T. Chugh, Y. Jin, K. Miettinen, J. Hakanen, and K. Sindhya, "A surrogate-assisted reference vector guided evolutionary algorithm for computationally expensive many-objective optimization," *IEEE Transactions on Evolutionary Computation*, vol. 22, no. 1, pp. 129–142, 2018.

[39] J. Knowles, "ParEGO: a hybrid algorithm with on-line landscape approximation for expensive multiobjective optimization problems," *IEEE Transactions on Evolutionary Computation*, vol. 10, no. 1, pp. 50–66, 2006.

[40] Q. Zhang, W. Liu, E. Tsang, and B. Virginas, "Expensive multiobjective optimization by MOEA/D with gaussian process model," *IEEE Transactions on Evolutionary Computation*, vol. 14, no. 3, pp. 456–474, 2010.

[41] W. Ponweiser, T. Wagner, D. Biermann, and M. Vincze, "Multiobjective optimization on a limited budget of evaluations using model-assisted $\mathcal{S}$-metric selection," in *International Conference on Parallel Problem Solving from Nature*. Springer, 2008, pp. 784–794.

[42] J. Zhang, A. Zhou, K. Tang, and G. Zhang, "Preselection via classification: A case study on evolutionary multiobjective optimization," *Information Sciences*, vol. 465, pp. 388–403, 2018.

[43] C.-W. Seah, Y.-S. Ong, I. W. Tsang, and S. Jiang, "Pareto rank learning in multi-objective evolutionary algorithms," in *2012 IEEE Congress on Evolutionary Computation*. IEEE, 2012, pp. 1–8.

[44] K. S. Bhattacharjee and T. Ray, "A novel constraint handling strategy for expensive optimization problems," in *11th World Congress on Structural and Multidisciplinary Optimization*, 2015.

[45] S. Bandaru, A. H. Ng, and K. Deb, "On the performance of classification algorithms for learning Pareto-dominance relations," in *2014 IEEE Congress on Evolutionary Computation (CEC)*. IEEE, 2014, pp. 1139–1146.

[46] L. Pan, C. He, Y. Tian, H. Wang, X. Zhang, and Y. Jin, "A classification-based surrogate-assisted evolutionary algorithm for expensive many-objective optimization," *IEEE Transactions on Evolutionary Computation*, vol. 23, no. 1, pp. 74–88, 2019.

[47] I. Giagkiozis and P. J. Fleming, "Increasing the density of available Pareto optimal solutions," *Automatic Control and Systems Engineering*, 2012.

[48] ——, "Pareto front estimation for decision making," *Evolutionary Computation*, vol. 22, no. 4, pp. 651–678, 2014.

[49] R. Cheng, Y. Jin, K. Narukawa, and B. Sendhoff, "A multiobjective evolutionary algorithm using Gaussian process-based inverse modeling," *IEEE Transactions on Evolutionary Computation*, vol. 19, no. 6, pp. 838–856, 2015.

[50] R. Cheng, M. Li, K. Li, and X. Yao, "Evolutionary multiobjective optimization-based multimodal optimization: Fitness landscape approximation and peak detection," *IEEE Transactions on Evolutionary Computation*, vol. 22, no. 5, pp. 692–706, 2018.

[51] T. J. Santner, B. J. Williams, W. Notz, and B. J. Williams, *The design and analysis of computer experiments*. Springer, 2003.

[52] C. M. Bishop, *Neural networks for pattern recognition*. Oxford university press, 1995.

[53] S. N. Lophaven, H. B. Nielsen, J. Søndergaard *et al.*, *DACE: a Matlab kriging toolbox*. Citeseer, 2002, vol. 2.

[54] K. Price, R. M. Storn, and J. A. Lampinen, *Differential evolution: a practical approach to global optimization*. Springer Science & Business Media, 2006.

[55] J. Dennis and V. Torczon, "Managing approximation models in optimization," *Multidisciplinary Design Optimization: State-of-the-art*, pp. 330–347, 1997.

[56] M. T. M. Emmerich, K. C. Giannakoglou, and B. Naujoks, "Single- and multiobjective evolutionary optimization assisted by gaussian random field metamodels," *IEEE Transactions on Evolutionary Computation*, vol. 10, no. 4, pp. 421–439, 2006.

[57] G. Yu, Y. Jin, and M. Olhofer, "Benchmark problems and performance indicators for search of knee points in multiobjective optimization," *IEEE Transactions on Cybernetics*, vol. 50, no. 8, pp. 3531–3544, 2020.

[58] Y. Tian, R. Cheng, X. Zhang, and Y. Jin, "PlatEMO: A matlab platform for evolutionary multi-objective optimization [educational forum]," *IEEE Computational Intelligence Magazine*, vol. 12, no. 4, pp. 73–87, 2017.

[59] E. Zitzler, M. Laumanns, and L. Thiele, "SPEA2: Improving the strength pareto evolutionary algorithm for multiobjective optimization," in *Evolutionary Methods for Design, Optimization and Control with Applications to Industrial Problems. Proceedings of the EUROGEN'2001. Athens. Greece, September 19-21*, 2001, pp. 95–100.

[60] R. B. Agrawal, K. Deb, and R. B. Agrawal, "Simulated binary crossover for continuous search space," *Complex Systems*, vol. 9, no. 3, pp. 115–148, 1994.

[61] K. Deb, K. Sindhya, and J. Hakanen, *Multi-Objective Optimization: Theory and Practice*. Decision Sciences, 2016.

[62] R. Cheng, T. Rodemann, M. Fischer, M. Olhofer, and Y. Jin, "Evolutionary many-objective optimization of hybrid electric vehicle control: From general optimization to preference articulation," *IEEE Transactions on Emerging Topics in Computational Intelligence*, vol. 1, no. 2, pp. 97–111, 2017.

[63] F. R. Salmasi, "Control strategies for hybrid electric vehicles: Evolution, classification, comparison, and future trends," *IEEE Transactions on vehicular technology*, vol. 56, no. 5, pp. 2393–2404, 2007.

[64] E. Zitzler and L. Thiele, "Multiobjective evolutionary algorithms: a comparative case study and the strength Pareto approach," *IEEE Transactions on Evolutionary Computation*, vol. 3, no. 4, pp. 257–271, 1999.

Guo Yu (M'20, IEEE) received the B.S. degree in information and computing science and the M.Eng. degree in computer technology from Xiangtan University, Xiangtan, China, in 2012 and 2015, respectively. He received the Ph.D. degree in computer science from University of Surrey, Guildford, U.K., in 2020.

He is currently a research fellow with the Key Laboratory of Smart Manufacturing in Energy Chemical Process, East China University of Science and Technology. His current research interests include evolutionary optimization and machine learning. Dr. Yu was a recipient of 2020 Shanghai "Super Postdoctoral" incentive Program and 2020 National Excellent Self-funded Student Scholarship. He is a member of IEEE, and a regular reviewer of more than 10 journals such as the IEEE Transaction on Evolutionary Computation, IEEE Transaction on Cybernetics, Artificial Intelligence, IEEE Computational Intelligence Magazine, IEEE Access, Complex & Intelligent Systems, Applied Soft Computing, and Soft Computing.

Yaochu Jin (Fellow, IEEE) received the B.Sc., M.Sc., and Ph.D. degrees in automatic control from Zhejiang University, Hangzhou, China, in 1988, 1991, and 1996, respectively, and the Dr.-Ing. degree from Ruhr-University Bochum, Bochum, Germany, in 2001.

He is presently an Alexander von Humboldt Professor for Artificial Intelligence endowed by the German Federal Ministry of Education and Research, Chair of Nature Inspired Computing and Engineering, Faculty of Technology, Bielefeld University, Germany, and a Distinguished Chair in Computational Intelligence, Department of Computer Science, University of Surrey, Guildford, U.K. He was a Finland Distinguished Professor funded by the Finnish Funding Agency for Innovation and a Changjiang Distinguished Visiting Professor appointed by the Ministry of Education, China. His main research interests include data-driven evolutionary optimization, trustworthy machine learning, multi-objective evolutionary learning, and evolutionary developmental systems.

Dr Jin is currently the Editor-in-Chief of the IEEE TRANSACTIONS ON COGNITIVE AND DEVELOPMENTAL SYSTEMS and the Editor-in-Chief of Complex & Intelligent Systems. He was the Vice President for Technical Activities of the IEEE Computational Intelligence Society and the General Co-Chair of the 2016 IEEE Symposium Series on Computational Intelligence and the Conference Chair 2020 IEEE Congress on Evolutionary Computation. He is the recipient of the 2018 and 2021 IEEE Transactions on Evolutionary Computation Outstanding Paper Award, and the 2015, 2017, and 2020 IEEE Computational Intelligence Magazine Outstanding Paper Award. He is named as a Highly Cited Researcher for 2019 and 2020 by the Web of Science Group. He is a Member of the Academia Europaea and Fellow of IEEE.

Markus Olhofer received the Dipl.-Ing. degree in electrical engineering and the Ph.D. degree in electrical engineering from Ruhr-University Bochum, Bochum, Germany, in 1997 and 2000, respectively.

He joined the Future Technology Research Division, Honda R&D Europe (Germany) GmbH, Offenbach, Germany, in 1998 and has been the Chief Scientist and the Head of the Complex Systems Optimization and Analysis Group, Honda Research Institute Europe, Offenbach, since 2010. He is a Visiting Professor with the Department of Computer Science, University of Surrey, Guildford, U.K. His current research interests include the extension of soft computing methods to meet requirements in complex engineering problems, ranging from evolutionary design optimization to engineering data mining.

Qiqi Liu received the B.Eng. degree in industrial engineering from the Xi'an University of Science and Technology, Xi'an, China, in 2013, and the M.E. degree in information and communication engineering from Shenzhen University, Shenzhen, China, in 2016. She is currently pursuing the Ph.D. degree in computer science with the University of Surrey, Guildford, U.K.

Her current research interests include evolutionary many-objective optimization, surrogate-assisted evolutionary optimization, and preference learning. Ms. Liu is a Regular Reviewer of Complex & Intelligent Systems, Soft Computing, and Swarm and Evolutionary Computation.

Wenli Du received the B.S. and M.S. degrees in chemical process control from the Dalian University of Technology, Dalian, China, in 1997 and 2000, respectively, and the Ph.D. degree in control theory and control engineering from the East China University of Science and Technology, Shanghai, China, in 2005.

She is currently a Professor of the College of Information Science and Engineering, East China University of Science and Technology, and is also the Vice Dean of the Key Laboratory of Smart Manufacturing in Energy Chemical Process, Ministry of Education, East China University of Science and Technology. Her current research interests include control theory and applications, system modeling, advanced control, and process optimization.